Eur. J. Mineral., 36, 687–708, 2024
https://doi.org/10.5194/ejm-36-687-2024

European Journal of Mineralogy
Open Access

Crystal chemistry of Belgian ardennites

Martin Depret[1], Frédéric Hatert[1], Michel Blondieau[2], Stéphane Puccio[3], Muriel M. L. Erambert[4], Fabrice Dal Bo[1], and Florent Bomal[1]

[1]Laboratory of Mineralogy B18, University of Liège, 4000 Liège, Belgium
[2]independent researcher: Val des Cloches 131, 6927 Tellin, Belgium
[3]independent researcher: Rue des Fontaines 156, 4041 Vottem, Belgium
[4]Department of Geosciences, University of Oslo, P.O. Box 1047 Blindern, 0316 Oslo, Norway

Correspondence: Martin Depret (martin.depret@uliege.be)

Received: 28 February 2024 – Revised: 1 July 2024 – Accepted: 16 July 2024 – Published: 30 August 2024

Abstract. The mineral ardennite-(As), which belongs to the *ardennite* group, was originally described in the locality of Salmchâteau, Stavelot Massif, Belgium. In the past 10 years, several new samples of ardennites have been found at seven localities of this region, motivating us to reinvestigate the crystal chemistry of the ardennite group. Under the polarizing microscope, most ardennites form lamellae or needles included in quartz veins or constituting the matrix of red Ordovician schists. Electron-microprobe analyses, as well as single-crystal structure refinements, show a homovalent substitution of As^{5+} by V^{5+} at the $T4$ tetrahedral site, leading to a complete solid solution between ardennite-(As) and ardennite-(V). Minor substitutions on that site allow the incorporation of a maximum of 0.28 P^{5+} atoms per formula unit (apfu) and of less than 0.1 Si^{4+} pfu, except in a sample from Arbrefontaine, where Si reaches 0.74 apfu. The main substitution mechanism, affecting both the $T4$ and $M3$ sites, is $^{T4}Si^{4+} + {}^{M3}(Al,Fe)^{3+} \leftrightarrow {}^{T4}(As,V,P)^{5+} + {}^{M3}Mg^{2+}$. Crystal-chemistry calculations indicate a positive correlation between the unit-cell parameters and the (Ca + Mg + Fe) contents of ardennites, as well as a negative correlation between the bond length distortion coefficients at the $T4$ and $M3$ sites. The existence of possible Si-rich and P-rich end-members, as well as the nomenclature of the ardennite group in which *dewalquite* could be revalidated, is discussed.

1 Introduction

The name *ardennite* was given to a rare Mn-rich aluminium silicate discovered in a quartz vein at Salmchâteau, Belgian Ardennes, during the second half of the 19th century. The samples were simultaneously investigated by Arnold von Lasaulx and Félix Pisani, who initially considered the species to be vanadium-bearing (von Lasaulx, 1872a, b; Pisani, 1872) and then considered it to be arsenic-rich (Pisani, 1873). The latter author decided to name the species *dewalquite*, in honour of the famous Belgian geologist Gustave Dewalque, while A. von Lasaulx named the mineral ardennite for the Ardennes region in Belgium where it was found. Due to historical priority, only the name ardennite was retained in the subsequent literature for both As- and V-bearing samples.

Recent guidelines of the Commission on New Minerals, Nomenclature and Classification (CNMNC) of the International Mineralogical Association (IMA) state that a new mineral species should be defined when a crystallographic site of the structure is dominantly occupied by a new constituent (Hatert and Burke, 2008). Consequently, Barresi et al. (2007) decided to define two distinct species in the ardennite solid solution: ardennite-(As) with the ideal formula $Mn_4^{2+}Al_4(AlMg)(AsO_4)(SiO_4)_2(Si_3O_{10})(OH)_6$ and with type locality Salmchâteau (Belgium) and ardennite-(V) with the ideal formula $Mn_4^{2+}Al_4(AlMg)(VO_4)(SiO_4)_2(Si_3O_{10})(OH)_6$ and with type locality Sparone (Piedmont, Italy). The ardennite group also includes the two isotypic minerals alpeite, $Ca_4Mn_2^{3+}Al_2(Mn^{3+}Mg)(VO_4)(SiO_4)_2(Si_3O_{10})(OH)_6$ (Kampf et al., 2017), and kannanite,

$Ca_4Al_4(AlMg)(VO_4)(SiO_4)_2(Si_3O_{10})(OH)_6$ (Nishio-Hamane et al., 2018).

Ardennite-(As) and ardennite-(V) occur in highly oxidized manganiferous metasediments that have been affected by low- to high-grade metamorphism (Pasero et al., 1994). Both minerals are stable from 300 to 600 °C and over a wide range of pressures (1–28 kbar), as shown by their occurrence in low-metamorphism environments (Kramm, 1982; Fransolet, 1982) as well as in greenschist (e.g. Nayak, 1967), blueschist (e.g. Reinecke and Hatzipanagiotou, 1987), and eclogite metamorphic facies (e.g. Dal Piaz et al., 1979; for a compilation, see Pasero et al., 1994).

The general formula of ardennite-group minerals may be written as $A_4M_6T_6O_{22}(OH)_6$, but several substitution mechanisms occur that explain the complex chemical compositions observed in some samples (Pasero et al., 1994). The large A sites mainly contain Mn^{2+} and smaller amounts of Ca and Mg; the octahedral M sites can host Al, Mg, Fe^{3+}, Mn^{3+}, and other minor cations; and the tetrahedral T sites are occupied by Si, As, V, and P (Donnay and Allmann, 1968; Barresi et al., 2007).

Ardennite is orthorhombic, with space group *Pmmn* and $a \approx 5.8$, $b \approx 18.6$, and $c \approx 8.8$ Å, and its crystal structure is formed by chains of edge-sharing octahedra running along the a axis ($M1$, $M2$, $M3$ octahedra), connected by SiO_4 ($T1$) and Si_3O_{10} groups (($T2$–$T3$–$T2$)O_{10}) (Donnay and Allmann, 1968; these authors used the *Pnmm* setting with $a \approx 8.8$, $b \approx 5.8$, and $c \approx 18.6$ Å). The large A cations ($A1$, $A2$) occur in 6-fold-coordination and 7-fold-coordination polyhedra located in cavities of the structure, and the $T4$ tetrahedra are connected to $M3$ and are occupied by pentavalent cations (As^{5+}, V^{5+}, P^{5+}), in contrast to the other T sites, which are occupied by Si^{4+}. The charge balance is compensated for by a coupled heterovalent substitution mechanism involving the $T4$ and $M3$ sites: $^{T4}Si^{4+} + {}^{M3}(Al, Fe)^{3+} \leftrightarrow {}^{T4}(As, V, P)^{5+} + {}^{M3}Mg^{2+}$. The general formula can therefore be written as $A_4^{2+}(M_5^{3+}M^{2+})(T_5^{4+}T^{5+})O_{22}(OH)_6$.

In Belgium, ardennite occurs on the southern border of the Stavelot-Venn Massif, closely associated with red to purple Mn- and Fe-rich slates of Ordovician age. Classic localities include Salmchâteau, the type locality of ardennite-(As), as well as Bierleux and Bihain (Fransolet, 1982; Pasero et al., 1994). During the past decades, several new occurrences of ardennite have been discovered in this area, initiating the extensive crystal-chemistry study presented in this paper. Our goal is to present the new structural and chemical data collected on 11 Belgian ardennite samples from different localities of the Stavelot Massif in order to better assess the cation distributions in these complex ardennite-group minerals.

2 Geological setting

The Stavelot-Venn Massif (SVM), Belgian Ardennes, is a Cambro-Ordovician inlier belonging to the Rhenohercynian zone of the Variscan orogenic belt (Fielitz and Mansy, 1999). The massif shows a continuous terrigenous sedimentation from lower Cambrian to Middle Ordovician (Geukens, 1986, 1999; Verniers et al., 2001) and is directly surrounded by discordant Lower Devonian conglomerates (Bultynck and Dejonghe, 2001; Fig. 1a). Lithostratigraphically, the Cambro-Ordovician rocks of the SVM are subdivided in three different groups: the Deville Group characterized by light-grey to greenish quartzites and slates of lower to middle Cambrian age, the Revin Group containing dark-grey to black slates and quartzites of upper Cambrian age, and the Salm Group composed of Ordovician rocks (Verniers et al., 2001).

The SVM was first affected by a very-low-grade metamorphism during the Caledonian orogeny. The highest-P–T conditions of 0.8–3 kbar and 280–380 °C have been identified in the southern part of the massif, based on fluid-inclusion measurements on quartz veins (Ferket et al., 1998). The area was then affected by a very-low-grade to low-grade Variscan metamorphism during the upper Carboniferous (Schreyer, 1975; Kramm, 1982; Kramm et al., 1985), which superimposed and completely overprinted the Caledonian metamorphism. Metamorphic minerals indicative of the P–T conditions are generally scarce in the region, except in the manganese-rich sediments of the Ottré Formation (Salm Group, Middle Ordovician). These rocks exhibit an unusual geochemistry related to hydrothermal exhalations that occurred during the sedimentation process (Krosse and Schreyer, 1993). Based on mineralogical assemblages involving andalusite, Mn-bearing chloritoid, and spessartine, as well as on white K-mica composition, Kramm (1982) estimated P–T conditions reaching 1.5–2 kbar and 360–420 °C in the southern part of the massif. In the Lienne Valley, lower-P–T conditions estimated at ∼ 300 °C and 1–2 kbar were constrained by the occurrence of carpholite (Theye et al., 1996).

Rocks of the Ottré Formation belong to the middle part of the Salm Group and are characterized by a significant enrichment in Fe and Mn. On the basis of their mineralogical contents, these rocks were subdivided into three lithostratigraphic members: the *Meuville* Member composed of red slates containing manganese oxides (mainly cryptomelane and lithiophorite), the *Les Plattes* Member characterized by purple andalusite-bearing slates containing layers of *coticule* (a creamy spessartine-bearing rock mined in the region for whetstones; Goemaere, 2007; Baijot et al., 2011), and the *Colanhan* Member formed by purple to greenish chloritoid-bearing slates (Verniers et al., 2001). These rocks mainly occur in the Salm and in the Lienne valleys, located at the south-eastern border and in the western part of the SVM, respectively (Fig. 1b).

The unusual geochemistry of these rocks, as well as the low-grade metamorphism that affected the region, produced a plethora of rare and crystallochemically complex minerals, for example ardennite-(As), ottrélite, davreuxite, and stavelotite-(La), for which the type localities are located in

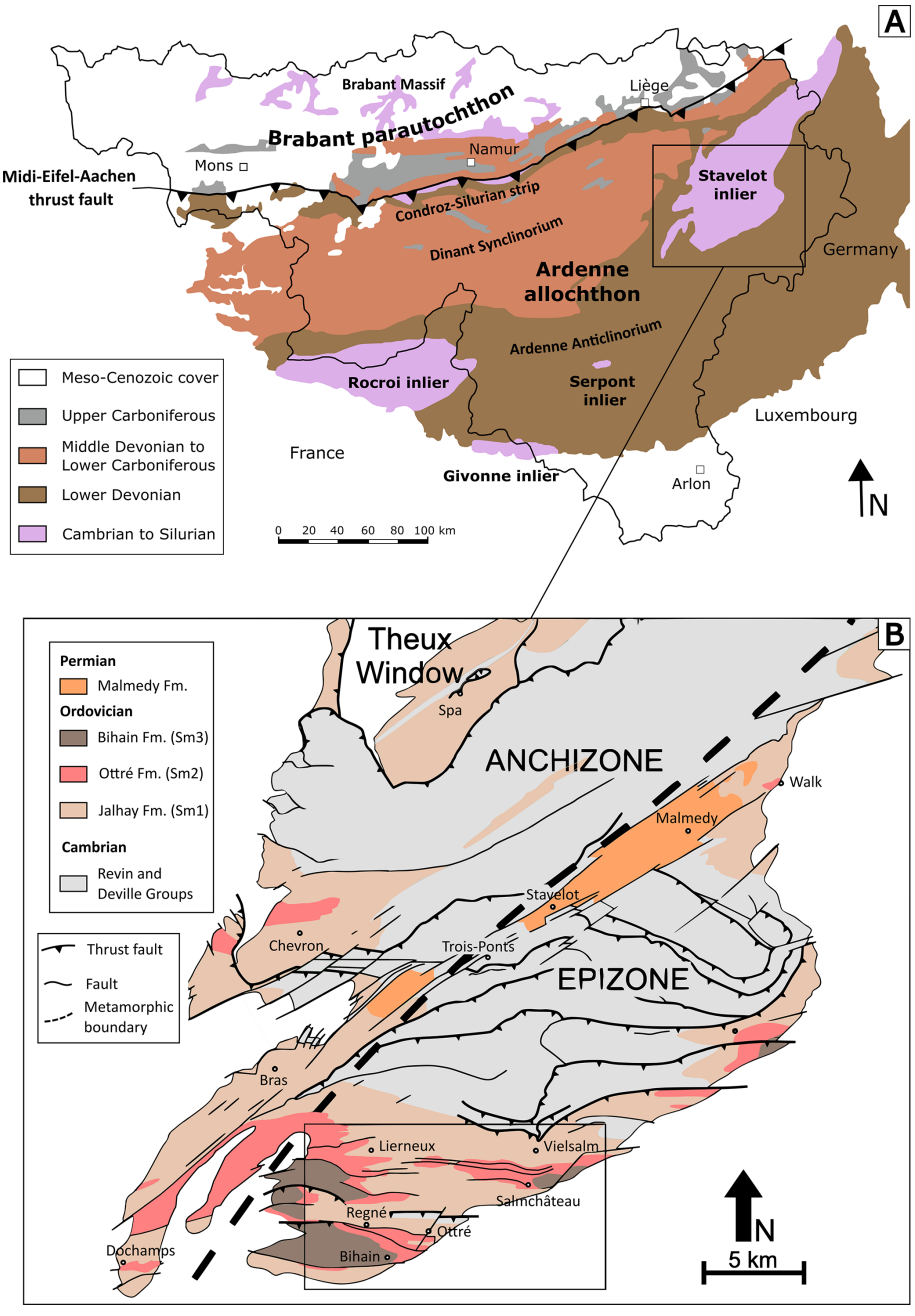

Figure 1. **(a)** Simplified geological map of southern Belgium, showing the position of the Cambro-Ordovician Stavelot-Venn Massif. **(b)** Geological map of the southern part of the Stavelot-Venn Massif, showing the position of the anchizone and the epizone. The region of the present study is shown with a rectangle, which includes the localities of Vielsalm, Salmchâteau, Ottré, Bihain, Regné, and Lierneux. Geology is according to Geukens (1986, 1999) and modified from Herbosch et al. (2016).

the SVM (Hatert et al., 2002; Bernhardt et al., 2005). In the Salm syncline, numerous quartz veins cross-cut these rocks, remobilizing exotic chemical elements and thus producing rare minerals as copper sulfides (Hatert, 2003, 2005), tellurides (Hatert, 1996; Hatert et al., 2002), and recently found malhmoodite and montanite (Blondieau et al., 2017). In the Lienne Valley, carpholite (Theye et al., 1996) and sursassite (Hatert et al., 2008), as well as numerous other species associated with a pyrolusite-rich manganese ore (Hatert et al., 2014), occur.

Table 1. Electron-microprobe analyses of ardennite samples from the Stavelot Massif. See Table 3 for information about the abbreviations used in sample names.

		TDM-1a	TDM-1b	TDP-1	REGN-1	SALM-1	SALM-2	SALM-3	CORX-1
SiO_2 (wt %)		28.23	28.95	27.88	28.19	28.82	28.38	27.81	28.65
As_2O_5		1.59	0.96	10.94	9.20	5.62	4.66	10.73	4.42
V_2O_5		7.38	8.48	0.17	0.41	3.71	4.77	0.32	4.25
P_2O_5		0.16	0.10	0.36	0.94	0.14	0.15	0.18	0.42
Al_2O_3		26.79	24.20	24.36	25.28	23.62	24.00	23.54	23.80
Fe_2O_3		0.82	0.87	0.68	0.52	0.96	0.75	1.71	0.78
Mn_2O_3*		–	–	–	–	0.83	0.75	–	0.90
V_2O_3		–	–	–	–	–	–	–	–
MnO		25.90	26.37	25.22	26.53	23.80	25.55	25.57	24.73
CaO		0.52	0.59	0.86	0.45	2.56	1.23	0.64	1.73
MgO		2.87	3.55	4.05	3.35	3.40	3.54	4.00	3.35
CuO		–	–	0.08	0.05	0.15	0.10	0.08	0.04
ZnO		0.01	–	0.06	0.05	0.02	0.04	0.05	0.04
H_2O*		5.46	5.43	5.19	5.25	5.19	5.16	5.12	5.18
Total		99.75	99.51	99.87	100.22	98.82	99.07	99.74	98.31
Cation numbers (apfu)									
*T*1, *T*2, *T*3	Si	4.854	5.000	4.866	4.888	5.000	4.944	4.878	5.000
	Al	0.146	–	0.134	0.112	–	0.056	0.122	–
	Σ	5.000	5.000	5.000	5.000	5.000	5.000	5.000	5.000
*T*4	Si	–	0.004	–	–	0.032	–	–	0.020
	As	0.143	0.086	0.999	0.834	0.513	0.425	0.984	0.405
	V^{5+}	0.838	0.969	0.020	0.047	0.428	0.549	0.038	0.492
	P	0.024	0.015	0.053	0.138	0.021	0.023	0.027	0.063
	Al	–	–	–	–	0.006	0.003	–	0.020
	Σ	1.005	1.074	1.072	1.019	1.000	1.000	1.049	1.000
*M*1, *M*2	Al	4.000	4.000	4.000	4.000	4.000	4.000	4.000	4.000
*M*3	Al	1.283	0.929	0.878	1.055	0.856	0.868	0.754	0.894
	Fe^{3+}	0.106	0.114	0.090	0.068	0.127	0.098	0.226	0.103
	Mn^{3+}	–	–	–	–	0.110	0.100	–	0.120
	V^{3+}	–	–	–	–	–	–	–	–
	Cu	–	–	0.010	0.007	0.019	0.014	0.010	0.006
	Zn	–	–	0.008	0.007	–	–	0.007	0.005
	Mg	0.611	0.914	1.014	0.863	0.886	0.919	1.003	0.872
	Ca	–	0.043	–	–	0.002	0.001	–	–
	Mn^{2+}	–	–	–	–	–	–	–	–
	Σ	2.000	2.000	2.000	2.000	2.000	2.000	2.000	2.000
*A*1, *A*2	Mn^{2+}	3.772	3.861	3.729	3.897	3.520	3.770	3.799	3.670
	Ca	0.096	0.066	0.162	0.083	0.476	0.228	0.120	0.326
	Mg	0.125	–	0.039	0.002	–	–	0.042	0.004
	Σ	3.993	3.927	3.930	3.982	3.996	3.998	3.961	4.000
OH		6.260	6.250	6.047	6.069	6.045	6.000	5.994	6.057

* Calculated values.

3 Analytical methods

Petrographic observations of ardennites were realized on thin sections with a Leica DM LP polarizing microscope, and electron-microprobe analyses were performed in the Department of Geosciences at the University of Oslo, Norway, using a Cameca SX100 instrument equipped with five wavelength-dispersive spectrometers (analyst Muriel M. L. Erambert). Analytical conditions were an accelerating voltage of 15 kV, a beam current of 15 nA, and

Table 1. Continued.

		BIHN-1	BIHN-2a	BIHN-2b	BIHN-2c	OTTR-1a	OTTR-1b	OTTR-1c	ARBR
SiO_2 (wt %)		28.27	27.60	28.81	28.89	29.65	29.59	28.26	33.33
As_2O_5		8.60	3.58	5.94	–	4.53	2.84	2.77	0.05
V_2O_5		1.66	4.56	1.83	7.36	2.66	3.00	4.90	2.04
P_2O_5		0.24	0.85	1.45	0.32	1.16	1.92	0.58	0.18
Al_2O_3		24.30	25.83	25.58	26.64	25.42	25.68	25.03	22.70
Fe_2O_3		0.67	0.57	0.55	0.09	0.62	0.64	0.54	0.70
Mn_2O_3*		–	–	–	–	–	–	–	–
V_2O_3		–	–	–	–	–	–	–	5.02
MnO		25.81	26.68	26.14	26.98	25.93	26.44	26.99	25.86
CaO		0.93	0.57	0.86	0.45	1.05	0.86	0.45	0.98
MgO		3.53	3.18	3.58	2.85	3.18	2.91	2.95	2.52
CuO		0.07	0.04	0.01	–	–	–	–	0.04
ZnO		0.04	0.11	0.09	0.07	0.08	0.05	0.07	0.09
H_2O*		5.18	5.06	5.21	5.21	5.29	5.30	5.12	4.92
Total		99.30	98.64	100.05	98.84	99.56	99.22	97.66	98.44
Cation numbers (apfu)									
*T*1, *T*2, *T*3	Si	4.948	4.793	4.936	4.965	5.000	5.000	4.962	5.000
	Al	0.052	0.207	0.064	0.035	–	–	0.038	–
	Σ	5.000	5.000	5.000	5.000	5.000	5.000	5.000	5.000
*T*4	Si	–	–	–	–	0.098	0.085	–	0.736
	As	0.787	0.325	0.532	–	0.407	0.255	0.254	0.004
	V^{5+}	0.192	0.524	0.207	0.836	0.303	0.341	0.568	0.232
	P	0.036	0.125	0.211	0.046	0.169	0.279	0.087	0.026
	Al	–	0.026	0.050	0.118	0.023	0.040	0.091	0.002
	Σ	1.015	1.000	1.000	1.000	1.000	1.000	1.000	1.000
*M*1, *M*2	Al	4.000	4.000	4.000	4.000	4.000	4.000	4.000	4.000
*M*3	Al	0.961	1.052	1.051	1.242	1.127	1.161	1.049	0.602
	Fe^{3+}	0.088	0.074	0.071	0.012	0.080	0.082	0.071	0.090
	Mn^{3+}	–	–	–	–	–	–	–	–
	V^{3+}	–	–	–	–	–	–	–	0.695
	Cu	0.010	0.006	–	–	–	–	–	0.005
	Zn	–	0.014	0.012	0.010	0.010	0.006	0.010	0.012
	Mg	0.920	0.824	0.866	0.730	0.783	0.744	0.772	0.596
	Ca	0.021	0.030	–	0.006	–	0.007	0.086	–
	Mn^{2+}	–	–	–	–	–	–	0.012	–
	Σ	2.000	2.000	2.000	2.000	2.000	2.000	2.000	2.000
*A*1, *A*2	Mn^{2+}	3.826	3.923	3.793	3.927	3.775	3.848	4.001	3.770
	Ca	0.153	0.076	0.158	0.077	0.194	0.151	–	0.181
	Mg	–	–	0.048	–	0.032	–	–	0.050
	Σ	3.979	3.999	3.999	4.004	4.001	3.999	4.001	4.001
OH		6.044	5.867	5.958	5.970	6.061	6.079	5.990	5.650

* Calculated values.

a beam diameter of 5–10 µm. The standards used were wollastonite (Si), pyrophanite (Mn), Durango apatite (P), vanadinite (V), willemite (Zn), synthetic $GaAsO_4$ (Ga), Al_2O_3 (Al), MgO (Mg), and pure metals (Fe, Cu). Cation numbers were calculated on the basis of 16 cations per formula unit (pfu), while the OH^- contents were calculated to maintain charge balance. Iron is considered Fe_2O_3, and manganese is considered MnO. However, when the (Ca + Mn) content exceeds 4 atoms per formula unit (apfu), the excess of manganese is considered Mn^{3+}, which will be preferentially incorporated in the larger and more distorted *M*3 site (Pasero et al., 1994; Table 1).

Single-crystal X-ray diffraction measurements were carried out in the Laboratory of Mineralogy, University of Liège, Belgium, with a Rigaku Xcalibur diffractometer using the Mo$K\alpha$ radiation ($\lambda = 0.71073$ Å) coupled with an EOS charge-coupled device (CCD) detector. Data were corrected for Lorentz, polarization, and absorption effects, the latter using an empirical method and the SCALE3 ABSPACK scaling algorithm included in the CrysAlis RED package (Oxford Diffraction, 2007). The crystal structures were determined with SHELXS and then were refined with the SHELXL program included in Olex2 (Sheldrick, 2008; Dolomanov et al., 2003). Scattering curves for neutral atoms, together with anomalous dispersion corrections, were taken from the International Tables for X-Ray Crystallography (Wilson, 1992). More details concerning data collection and crystal structure refinements are given in Table 2.

Infrared spectra were obtained on a Thermo Nicolet Nexus 470 FTIR spectrometer with a 1 cm^{-1} resolution, covering the 400–4000 cm^{-1} range. The samples were prepared by mixing 2 mg of sample with 48 mg of KBr; the mixture was then compressed to form a pellet, which was dried for a few hours at 110 °C. In order to prevent contamination by atmospheric water, the measurements were performed under a dry air purge.

4 Sampling and petrographic description

Ardennite frequently forms prismatic crystals elongated on [100] and flattened on {001}, with a good (010) cleavage. In the SVM, it generally occurs as lamellar to bladed aggregates reaching several centimetres in diameter or as small isolated grains (less than 1 mm in length) randomly distributed in the quartz veins or in the host schists located at the contact point with those veins. Corin (1927) observed that ardennite appears to be a major constituent of the schists at the direct contact point with the ardennite-bearing quartz veins and becomes less abundant or completely disappears where the schists do not contain quartz veins. The samples studied in the present paper show that ardennite is not restricted to a single assemblage but that it can occur in various complex mineralogical and petrographic associations (Table 3).

Ardennite was initially found at Salmchâteau, in association with albite and *apatite* in relatively homogenous quartz veins. The most spectacular samples were extracted from this occurrence, where the prismatic ardennite crystals can reach 10 cm in length (Fig. 2a). In the same locality, ardennite has also been observed in more complex quartz veins containing muscovite, clinochlore, spessartine, hematite, albite, and apatite (SALM-1) or in very oxidized rocks containing albite, hollandite–strontiomelane, and braunite (SALM-2, CORX-1). In all these assemblages, ardennite frequently forms lenticular crystals, which had already been observed in thin sections by Cesàro and Abraham (1909) (Fig. 2b). In Thier del Preu, some andalusite-bearing quartz veins contain elongated ardennite prisms in close association with reddish hematite-rich quartz patches (TDP-1, Fig. 2c).

In the Bihain region, ardennite has been found in relatively pure quartz veins comparable to those of the type locality but containing minor patches of manganese oxides. But the mineral has also been observed with quartz, spessartine, hematite, and manganese oxides in thin veins (0.5–1 cm thickness) that cross-cut purple schists (BIHN-1), as well as in some fractures of whitish to greyish quartz-rich coticules (BIHN-2). In Ottré, located a few kilometres away, small grains of ardennite associated with vantasselite have been identified on the cleavage plane of a schist containing kaolinized spots of andalusite (OTTR-1). Ardennite from Thier du Mont (TDM-1) is developed on whitish quartz-rich coticules, showing a more complex association with quartz, greenish to yellowish spessartine, clinochlore, and hematite.

Rare reddish granular rocks containing red ardennite have been discovered in a few localities of the SVM. In Regné, these rocks are composed of abundant orange ardennite needles reaching 500 µm in length, associated with hematite grains (Fig. 2d, REGN-1). Frequently, thin quartz veins cross-cut these rocks and contain acicular crystals of ardennite (100–3200 µm) growing perpendicularly to the walls (Fig. 2e, REGN-1). In Salmchâteau, another rock containing well-developed red crystals of ardennite has been sampled (SALM-3), which is composed of muscovite, albite, hematite, spessartine, and minor quartz. Ardennite forms elongated crystals of 0.5–1 mm in those rocks and seems to be intimately associated with hematite.

Finally, ardennite has also been identified in coticule veins, which are composed of fine-grained spessartine grains (5–20 mm in diameter) dispersed in a matrix that is essentially formed by muscovite with minor quartz and chlorite (Kramm, 1976; Lessuise, 1980; Krosse and Schreyer, 1993). In those veins, ardennite forms millimetre-sized spots that show a typical granular texture (Fig. 2f); such textures were observed in several localities, for example in Thier del Preu, in Arbrefontaine, and in Bihain.

5 Crystal structure refinements

Crystal structure refinements were performed in space group *Pmmn*, and the unit-cell parameters (Table 2) are similar to those of the Belgian ardennite samples investigated by Pasero et al. (1994). Cation occupancies were refined considering Mn in the $A1$ and $A2$ sites; Al in the $M1$ and $M2$ sites; Mg in the $M3$ site; Si in the $T1$, $T2$, and $T3$ sites; and As in the $T4$ site. The occupancies of the O sites were constrained to 1, and the refined occupancies of the cation sites were used to calculate the refined site-scattering values. In the last refinement cycles, all atoms except hydrogen were refined with anisotropic displacement parameters. Atomic coordinates, cation occupancies, and anisotropic displacement parameters, as well as bond distances and angles, are available

Table 2. Data collection and structure refinement details for ardennites from the Stavelot Massif, Belgium.

	TDP-1	TDM-1	REGN-1	SALM-1	SALM-2	SALM-3
Crystal dimensions (mm)	0.43 × 0.15 × 0.06	0.22 × 0.19 × 0.10	0.20 × 0.11 × 0.05	0.47 × 0.29 × 0.14	0.35 × 0.25 × 0.17	0.46 × 0.25 × 0.14
a (Å)	5.798(1)	5.798(3)	5.799(2)	5.802(3)	5.807(2)	5.805(5)
b (Å)	18.477(5)	18.474(7)	18.467(7)	18.501(1)	18.510(8)	18.504(1)
c (Å)	8.695(2)	8.687(4)	8.689(3)	8.704(5)	8.696(3)	8.708(7)
V (Å^3)	931.52(4)	930.48(7)	930.58(6)	934.31(9)	934.84(7)	935.42(1)
Space group	*Pmmn*	*Pmmn*	*Pmmn*	*Pmmn*	*Pmmn*	*Pmmn*
Z	2	2	2	2	2	2
Operating conditions	40 kV, 40 mA	40 kV, 40 mA	40 kV, 40 mA	40 kV, 40 mA	40 kV, 40 mA	40 kV, 40 mA
Scan mode	ϕ/ω scan	ϕ/ω scan	ϕ/ω scan	ϕ/ω scan	ϕ/ω scan	ϕ/ω scan
$2\theta_{max}$	57.76°	58.15°	58.03°	57.81°	57.96°	57.89°
Range of indices	$-7 \le h \le 7$ $-25 \le k \le 21$ $-10 \le l \le 11$	$-7 \le h \le 7$ $-24 \le k \le 23$ $-7 \le l \le 11$	$-5 \le h \le 7$ $-20 \le k \le 23$ $-11 \le l \le 10$	$-7 \le h \le 7$ $-23 \le k \le 19$ $-10 \le l \le 11$	$-7 \le h \le 7$ $-23 \le k \le 15$ $-11 \le l \le 11$	$-7 \le h \le 7$ $-24 \le k \le 25$ $-10 \le l \le 11$
Measured intensities	7124	6998	6904	6872	7356	6978
Unique reflections	1286	1318	1281	1305	1307	1308
Independent non-zero ($I > 2\sigma(I)$) reflections	1233	1208	1191	1227	1240	1174
μ (mm^{-1})	5.169	5.411	5.174	5.153	5.386	3.21
Refined parameters	135	135	135	135	135	135
R_1 ($F_O > 2\sigma(F_O)$)	0.0204	0.0278	0.0195	0.0284	0.0181	0.0483
R_1 (all)	0.0214	0.0317	0.0224	0.0312	0.0194	0.0533
wR_2 (all)	0.0572	0.0743	0.0512	0.0698	0.0472	0.1276
S (goodness of fit)	1.181	1.314	1.070	1.090	1.125	1.089
Max peak and hole in the final ΔF map (e Å^{-3})	+0.61 and −0.96	+0.87 and −1.02	+0.37 and −0.53	+0.73 and −0.92	+0.43 and −0.59	+1.71 and −0.99

	BIHN-1	BIHN-2	CORX-1	OTTR-1
Crystal dimensions (mm)	0.15 × 0.09 × 0.04	0.13 × 0.10 × 0.08	0.27 × 0.20 × 0.14	0.15 × 0.08 × 0.07
a (Å)	5.804(4)	5.803(3)	5.810(1)	5.799(2)
b (Å)	18.479(1)	18.511(8)	18.506(3)	18.506(7)
c (Å)	8.696(5)	8.698(4)	8.703(1)	8.692(4)
V (Å^3)	932.59(1)	934.34(8)	935.71(3)	932.77(7)
Space group	*Pmmn*	*Pmmn*	*Pmmn*	*Pmmn*
Z	2	2	2	2
Operating conditions	40 kV, 40 mA	40 kV, 40 mA	40 kV, 40 mA	40 kV, 40 mA
Scan mode	ϕ/ω scan	ϕ/ω scan	ϕ/ω scan	ϕ/ω scan
$2\theta_{max}$	57.506	57.374	65.052	58.182
Range of indices	$-7 \le h \le 7$ $-24 \le k \le 14$ $-11 \le l \le 11$	$-7 \le h \le 4$ $-23 \le k \le 23$ $-11 \le l \le 11$	$-8 \le h \le 8$ $-26 \le k \le 27$ $-12 \le l \le 13$	$-7 \le h \le 7$ $-23 \le k \le 25$ $-11 \le l \le 11$
Measured intensities	6839	6856	29407	11805
Unique reflections	1303	1292	1835	1319
Independent non-zero ($I > 2\sigma(I)$) reflections	954	1088	1764	1180
μ (mm^{-1})	5.163	5.389	5.381	5.398
Refined parameters	135	135	135	135
R_1 ($F_O > 2\sigma(F_O)$)	0.0504	0.0370	0.0192	0.0340
R_1 (all)	0.0786	0.0489	0.0206	0.0403
wR_2 (all)	0.01239	0.0948	0.0538	0.0875
S (goodness of fit)	1.064	1.129	1.161	1.069
Max peak and hole in the final ΔF map (e Å^{-3})	+1.16 and −0.92	+0.75 and −0.80	+0.62 and −0.75	+0.79 and −0.71

in the Supplement (Tables S1 to S3). Average bond lengths are given in Table 4.

The ardennite structure is based on three types of chains composed of edge-sharing octahedra and aligned parallel to the a axis (Fig. 3a). The $M1$ and $M2$ chains occupied by Al are connected via corner-sharing tetrahedra to form planes perpendicular to the b axis, and the $M3$ chain occupied by Mg is located at positions that are intermediate between those planes (Fig. 3b). The large $A1O_6$ and $A2O_7$ polyhedra are occupied by manganese and are strongly distorted (Fig. 4).

Table 3. Ardennite samples investigated in the present paper: their provenance, associated minerals, petrographic description, and stratigraphic position.

Samples	Locality	Coordinates	Main associated minerals*	Sample description	Lithostratigraphy
TDP-1	Thier del Preu (Sart, Lierneux)	50.27971° N, 5.84334° E	Qz, Hem, Clc, Sud, ± And	Well-formed bladed yellow grains (up to 5 mm) in quartz veins with reddish quartz inclusions	Les Plattes
TDM-1	Thier du Mont (Sart, Lierneux)	50.27753° N, 5.88424° E	Qz, Sps, Clc, ± Hem	Orange to brownish grains (< 2 mm) on quartz-rich white-grey coticules	Les Plattes
REGN-1	Regné (coticule quarry)	50.24964° N, 5.79719° E	Qz, Hem, Clc, ± And	Yellow to red needles (< 3 mm) forming thin veins in ardennite-bearing reddish rocks	Les Plattes
SALM-1	Salmchâteau (railway bridge)	50.26845° N, 5.90749° E	Qz, Ms, Clc, Sps, Hem, Ab, Ap	Yellow to orange grains (< 1 mm) in quartz	Meuville
SALM-2	Salmchâteau (river)	50.26910° N, 5.90884° E	Qz, Ab, Hol	Yellow to orange grains sometimes reaching 2 mm in albite-bearing quartz	Meuville
SALM-3	Salmchâteau (railway bridge)	50.26845° N, 5.90751° E	Qz, Ms, Ab, Hem, Sps	Elongated red grains (0.5–1 mm) in reddish rocks	Meuville
BIHN-1	Bihain (Old manganese mine)	50.24613° N, 5.814719° E	Qz, Ms, Hem, Sps	Tiny yellow grains (< 200 µm) in thin quartz veins cross-cutting purple schists	Meuville
BIHN-2	Bihain (Vantasselite type locality)	50.24575° N, 5.81010° E	Qz, Clc	Tiny light-yellow grains (< 600 µm) on quartz-rich white-grey coticules	Les Plattes
CORX-1	Coreux (Salmchâteau)	50.27071° N, 5.90502° E	Qz, Ab, Hol, Sml, Bnt	Bladed orange to brown grains (< 2 mm) on quartz	Meuville
OTTR-1	Ottré (Ottré quarry)	50.24704° N, 5.82745° E	Vts, Hem	Yellow to slightly brown grains (< 150 µm) on purple schists	Les Plattes
ARBR-1	Arbrefontaine (Sart, Lierneux)	50.28330° N, 5.83799° E	Qz, Sps	Yellow to brown granular aggregates in quartz-rich coticules	Les Plattes

* Mineral symbols according to Warr (2021).

Two $A1O_6$ octahedra are connected together by one edge to form a dimer, which is connected by edge sharing to the $M3$ octahedra and by corner sharing to the $M2$ octahedra and to the $T4$ tetrahedron (Fig. 3). A second dimer, composed of two edge-sharing $A2O_7$ polyhedra, is connected by edge sharing to the $M1$ and $M3$ octahedra.

The most amazing feature of the ardennite structure consists in a trimer parallel to the b axis, formed by three corner-sharing $T2$ and $T3$ tetrahedra (Fig. 3). Three basal oxygens of the $T2$ tetrahedra belonging to those chains, as well as three basal oxygens of the isolated $T1$ tetrahedra, bridge the $M1$ and $M2$ octahedral chains together. The isolated $T4$ tetrahedron, containing pentavalent cations, is not connected to the $M1$–$M2$ planes but shares its corners with the $M3$ and $A1O_6$ octahedra (Fig. 3). The structural formula, deduced from these data, can be written as $A1_2A2_2(M1_2M2_2M3_2)(T1_2T2_2T3T4)O_{22}(OH)_6$.

For each crystallographic site, bond valence sums were calculated from the observed bond distances, using the empirical parameters of Brown and Altermatt (1985). Cation distributions were then accurately adjusted in order to reach the best fit between the refined site-scattering (RSS) and calculated site-scattering (CSS) values, the refined mean bond length (MBL) and calculated bond length (CBL) values, and the theoretical valence (TV) sums and calculated bond valence (BV) sums, taking into account the global chemical composition obtained from the electron-microprobe data (Table 1). The final assigned site populations (ASP), as well as all parameters deduced from the calculations mentioned above, are given in Table 5. Formulae deduced from the ASP

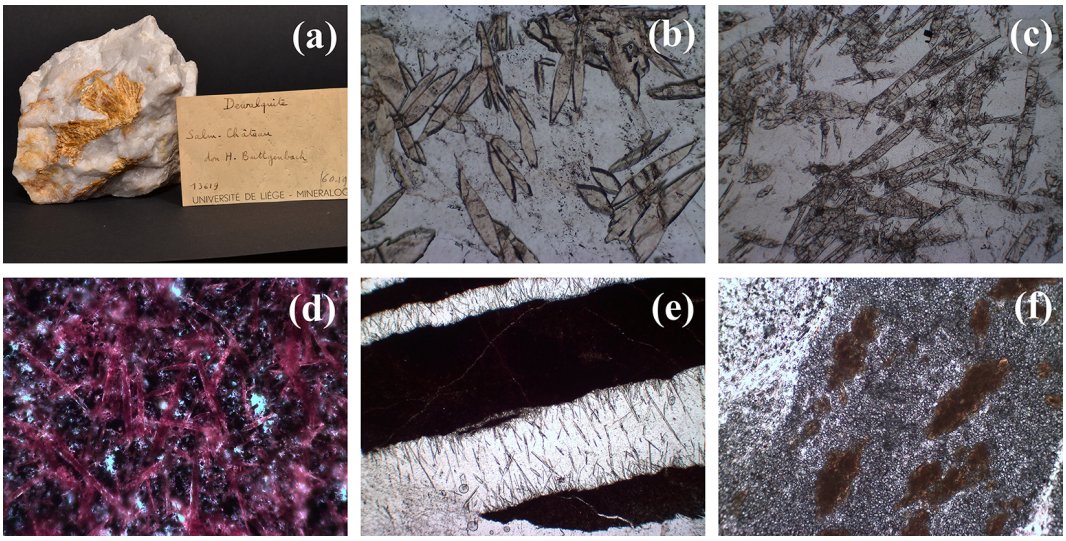

Figure 2. **(a)** Ardennite sample from Salmchâteau, the type locality of ardennite-(As). The mineral forms elongated and platy yellow crystals that reach 3 cm in length and are deposited on milky quartz. On the label, the mineral is still called "dewalquite", which was the name given by Pisani (1873) to the species. Collection of the Laboratory of Mineralogy, ULiège, no. 13619. **(b)** Lenticular shape of ardennite crystals, frequently observed in thin sections. Sample REGN-2, plane-polarized light microscopy, length of the photograph = 1.8 mm. **(c)** Ardennite from the Thier del Preu quarry, showing elongated crystals reaching 2 mm and included in quartz. Sample TDP-1, plane-polarized light microscopy, length of the photograph = 4.5 mm. **(d)** Orange to pink ardennite needles, major constituent of the red rock occurring at the contact point with ardennite-bearing quartz veinlets at Regné. Sample REGN-1, plane-polarized light microscopy, length of the photograph = 1.8 mm. **(e)** Quartz veinlets containing ardennite needles and cross-cutting the red ardennite-bearing rocks of Regné. Sample REGN-1, plane-polarized light microscopy, length of the photograph = 4.5 mm. **(f)** Granular ardennite aggregates observed in a coticule vein from Ottré. Sample COT-1, plane-polarized light microscopy, length of the photograph = 1.8 mm.

Table 4. Mean bond length (MBL) and bond length distortion (BLD) values for the cationic sites of Belgian ardennites.

	TDP-1		TDM-1		REGN-1		SALM-1		SALM-2	
Site	MBL	BLD	MBL	BLD	MBL	BLD	MBL	BLD	MBL	BLD
*A*1	2.244	5.399	2.240	4.599	2.245	5.213	2.244	5.207	2.244	4.788
*A*2	2.289	3.923	2.285	3.984	2.289	3.850	2.290	3.978	2.292	3.668
*M*1	1.899	1.196	1.900	1.310	1.899	1.249	1.900	1.241	1.899	1.253
*M*2	1.916	2.637	1.915	2.449	1.915	2.568	1.918	2.700	1.918	2.732
*M*3	1.993	3.347	1.984	2.801	1.991	3.320	1.998	3.348	1.996	3.080
*T*1	1.636	0.910	1.636	0.993	1.637	0.858	1.648	0.900	1.636	0.935
*T*2	1.630	1.279	1.628	1.229	1.629	1.138	1.639	1.388	1.629	1.262
*T*3	1.647	0.061	1.658	0.000	1.653	0.060	1.632	0.030	1.650	0.000
*T*4	1.687	1.927	1.710	2.924	1.674	2.210	1.693	1.979	1.702	2.526
	SALM-3		BIHN-1		BIHN-2		CORX-1		OTTR-1	
Site	MBL	BLD	MBL	BLD	MBL	BLD	MBL	BLD	MBL	BLD
*A*1	2.247	5.275	2.240	4.889	2.242	5.399	2.244	4.657	2.248	4.967
*A*2	2.292	3.842	2.291	3.664	2.289	3.923	2.290	3.809	2.291	3.732
*M*1	1.901	1.286	1.902	1.215	1.901	1.196	1.900	1.299	1.901	1.227
*M*2	1.919	2.791	1.920	2.431	1.916	2.637	1.917	2.586	1.914	2.473
*M*3	1.999	3.313	1.982	2.994	1.984	3.347	1.992	2.956	1.989	3.117
*T*1	1.637	0.947	1.639	1.106	1.642	1.081	1.639	0.948	1.640	0.976
*T*2	1.632	1.257	1.631	0.858	1.632	1.027	1.631	1.213	1.631	1.334
*T*3	1.650	0.182	1.668	0.540	1.672	0.090	1.657	0.012	1.659	0.030
*T*4	1.690	1.924	1.696	2.507	1.697	1.927	1.711	2.768	1.678	2.534

https://doi.org/10.5194/ejm-36-687-2024

Table 5. Assigned site population (ASP) information for the crystallographic sites of ardennites from the Stavelot Massif. These populations were calculated to reach the best fits between the refined site-scattering (RSS) and the calculated site-scattering (CSS) values, between the bond valence (BV) and the theoretical valence (TV) sums, and between the chemical formulae obtained from the crystal structure (STR) and from the electron-microprobe data (EMP).

	TDP-1					TDM-1				
Site	ASP	RSS	CSS	TV	BV	ASP	RSS	CSS	TV	BV
*A*1	0.95 Mn^{2+} + 0.05 Mg	24.00	24.35	2.00	1.85	0.95 Mn^{2+} + 0.05 Mg	24.35	24.35	2.00	1.84
*A*2	0.92 Mn^{2+} + 0.08 Ca	24.15	24.60	2.00	1.96	0.95 Mn^{2+} + 0.05 Ca	24.00	24.75	2.00	1.96
*M*1	1.00 Al	12.91	13.00	3.00	3.08	1.00 Al	12.72	13.00	3.00	3.07
*M*2	1.00 Al	13.03	13.00	3.00	2.97	1.00 Al	12.84	13.00	3.00	2.97
*M*3	0.55 Al + 0.45 Mg	12.74	12.55	2.55	2.56	0.60 Al + 0.35 Mg + 0.05 Fe^{3+}	12.67	13.30	2.65	2.51
*T*4	0.95 As + 0.05 P	31.55	32.10	5.00	4.89	0.85 V + 0.10 As + 0.05 P	23.25	23.60	5.00	5.01
EMP	$(Mn_{3.73}Ca_{0.16})(Al_{5.01}Mg_{1.05}Fe^{3+}_{0.09})(Si_{4.87})(As_{1.00}P_{0.05}V_{0.02})O_{22}(OH)_{6.00}$					$(Mn_{3.77}Ca_{0.10})(Al_{5.43}Mg_{0.74}Fe^{3+}_{0.11})(Si_{4.85})(V_{0.84}As_{0.14}P_{0.02})O_{22}(OH)_{6.00}$				
STR	$(Mn_{3.74}Ca_{0.16})(Al_{5.10}Mg_{1.00})(Si_{5.00})(As_{0.95}P_{0.05})O_{22}(OH)_{6.00}$					$(Mn_{3.80}Ca_{0.10})(Al_{5.20}Mg_{0.80}Fe^{3+}_{0.10})(Si_{5.00})(V_{0.85}As_{0.10}P_{0.05})O_{22}(OH)_{6.00}$				
	SALM-1					SALM-2				
Site	ASP	RSS	CSS	TV	BV	ASP	RSS	CSS	TV	BV
*A*1	1.00 Mn^{2+}	23.78	25.00	2.00	1.87	1.00 Mn^{2+}	24.33	25.00	2.00	1.85
*A*2	0.80 Mn^{2+} + 0.20 Ca	23.58	24.00	2.00	2.07	0.90 Mn^{2+} + 0.10 Ca	23.85	24.50	2.00	1.96
*M*1	1.00 Al	12.64	13.00	3.00	3.07	1.00 Al	12.73	13.00	3.00	3.07
*M*2	1.00 Al	12.91	13.00	3.00	2.96	1.00 Al	13.13	13.00	3.00	2.95
*M*3	0.45 Al + 0.45 Mg + 0.05 Fe^{3+} + 0.05 Mn^{3+}	12.70	13.80	2.55	2.60	0.45 Al + 0.45 Mg + 0.05 Fe^{3+} + 0.05 Mn^{3+}	13.09	13.80	2.55	2.60
*T*4	0.60 As + 0.40 V	30.62	29.00	5.00	5.11	0.55 V + 0.40 As + 0.05 P	25.54	26.60	5.00	4.96
EMP	$(Mn_{3.63}Ca_{0.48})(Al_{4.86}Mg_{0.89}Fe^{3+}_{0.13})(Si_{5.03})(As_{0.51}V_{0.43}P_{0.02})O_{22}(OH)_{6.00}$					$(Mn_{3.87}Ca_{0.23})(Al_{4.93}Mg_{0.92}Fe^{3+}_{0.10})(Si_{4.94})(V_{0.55}As_{0.42}P_{0.02})O_{22}(OH)_{6.00}$				
STR	$(Mn_{3.70}Ca_{0.40})(Al_{4.90}Mg_{0.90}Fe^{3+}_{0.10})(Si_{5.00})(As_{0.60}V_{0.40})O_{22}(OH)_{6.00}$					$(Mn_{3.90}Ca_{0.20})(Al_{4.90}Mg_{0.90}Fe^{3+}_{0.10})(Si_{5.00})(V_{0.55}As_{0.40}P_{0.05})O_{22}(OH)_{6.00}$				
	REGN-1					BIHN-1				
Site	ASP	RSS	CSS	TV	BV	ASP	RSS	CSS	TV	BV
*A*1	1.00 Mn^{2+}	24.23	25.00	2.00	1.87	1.00 Mn^{2+}	24.18	25.00	2.00	1.88
*A*2	0.95 Mn^{2+} + 0.05 Ca	23.93	24.75	2.00	1.93	0.90 Mn^{2+} + 0.10 Ca	24.10	24.50	2.00	1.97
*M*1	1.00 Al	12.69	13.00	3.00	3.08	1.00 Al	12.71	13.00	3.00	3.05
*M*2	1.00 Al	12.69	13.00	3.00	2.97	1.00 Al	12.71	13.00	3.00	2.93
*M*3	0.55 Al + 0.45 Mg	12.40	12.55	2.55	2.57	0.55 Al + 0.45 Mg	12.38	12.55	2.55	2.63
*T*4	0.80 As + 0.13 P + 0.07 V	27.92	29.96	5.00	4.94	0.70 As + 0.30 V	26.50	30.00	5.00	5.03
EMP	$(Mn_{3.90}Ca_{0.08})(Al_{5.17}Mg_{0.87}Fe^{3+}_{0.07})(Si_{4.89})(As_{0.83}P_{0.14}V_{0.05})O_{22}(OH)_{6.00}$					$(Mn_{3.83}Ca_{0.17})(Al_{5.01}Mg_{0.92}Fe^{3+}_{0.09})(Si_{4.95})(As_{0.79}V_{0.19}P_{0.04})O_{22}(OH)_{6.00}$				
STR	$(Mn_{3.90}Ca_{0.10})(Al_{5.10}Mg_{0.90})(Si_{5.00})(As_{0.80}P_{0.13}V_{0.07})O_{22}(OH)_{6.00}$					$(Mn_{3.80}Ca_{0.20})(Al_{5.10}Mg_{0.90})(Si_{5.00})(As_{0.70}V_{0.30})O_{22}(OH)_{6.00}$				

Table 5. Continued.

	SALM-3					CORX-1				
Site	ASP	RSS	CSS	TV	BV	ASP	RSS	CSS	TV	BV
*A*1	0.95 Mn^{2+} + 0.05 Mg	23.90	24.35	2.00	1.84	1.00 Mn^{2+}	24.28	25.00	2.00	1.85
*A*2	0.95 Mn^{2+} + 0.05 Ca	23.68	24.75	2.00	1.91	0.85 Mn^{2+} + 0.15 Ca	23.78	24.25	2.00	2.02
*M*1	1.00 Al	12.87	13.00	3.00	3.06	1.00 Al	12.78	13.00	3.00	3.07
*M*2	1.00 Al	13.00	13.00	3.00	2.95	1.00 Al	13.00	13.00	3.00	2.96
*M*3	0.45 Al + 0.45 Mg + 0.1 Fe^{3+}	13.06	13.85	2.55	2.60	0.45 Al + 0.45 Mg + 0.05 Fe^{3+} + 0.05 Mn^{3+}	13.04	13.80	2.55	2.63
*T*4	0.90 As + 0.10 V	31.61	32.00	5.00	5.00	0.60 V + 0.40 As	25.44	27.00	5.00	4.98
EMP	$(Mn_{3.80}Ca_{0.12})(Al_{4.87}Mg_{1.04}Fe^{3+}_{0.23})(Si_{4.88})(As_{0.98}V_{0.04}P_{0.03})O_{22}(OH)_{6.00}$					$(Mn_{3.79}Ca_{0.33})(Al_{4.91}Mg_{0.88}Fe^{3+}_{0.10})(Si_{5.02})(V_{0.49}As_{0.40}P_{0.06})O_{22}(OH)_{6.00}$				
STR	$(Mn_{3.80}Ca_{0.10})(Al_{4.90}Mg_{1.00}Fe^{3+}_{0.20})(Si_{5.00})(As_{0.90}V_{0.10})O_{22}(OH)_{6.00}$					$(Mn_{3.80}Ca_{0.30})(Al_{4.90}Mg_{0.90}Fe^{3+}_{0.10})(Si_{5.00})(V_{0.60}As_{0.40})O_{22}(OH)_{6.00}$				
	BIHN-2					OTTR-1				
Site	ASP	RSS	CSS	TV	BV	ASP	RSS	CSS	TV	BV
*A*1	1.00 Mn^{2+}	24.53	25.00	2.00	1.86	1.00 Mn^{2+}	24.23	25.00	2.00	1.84
*A*2	0.95 Mn^{2+} + 0.05 Ca	24.30	24.75	2.00	1.93	0.92 Mn^{2+} + 0.08 Ca	23.98	24.60	2.00	1.94
*M*1	1.00 Al	12.87	13.00	3.00	3.06	1.00 Al	12.75	13.00	3.00	3.06
*M*2	1.00 Al	12.74	13.00	3.00	2.96	1.00 Al	12.74	13.00	3.00	2.98
*M*3	0.60 Al + 0.40 Mg	12.60	12.60	2.60	2.59	0.60 Al + 0.40 Mg	12.76	12.60	2.60	2.57
*T*4	0.85 V + 0.15 P	22.95	21.80	5.00	4.99	0.40 V + 0.40 As + 0.20 P	25.58	25.40	5.00	4.92
EMP	$(Mn_{3.93}Ca_{0.08})(Al_{5.40}Mg_{0.73}Fe^{3+}_{0.01})(Si_{4.96})(V_{0.84}P_{0.05})O_{22}(OH)_{6.00}$					$(Mn_{3.78}Ca_{0.19})(Al_{5.15}Mg_{0.81}Fe^{3+}_{0.08})(Si_{5.10})(As_{0.41}V_{0.30}P_{0.17})O_{22}(OH)_{6.00}$				
STR	$(Mn_{3.90}Ca_{0.10})(Al_{5.20}Mg_{0.80})(Si_{5.00})(V_{0.85}P_{0.15})O_{22}(OH)_{6.00}$					$(Mn_{3.84}Ca_{0.16})(Al_{5.20}Mg_{0.80})(Si_{5.00})(As_{0.40}V_{0.40}P_{0.20})O_{22}(OH)_{6.00}$				

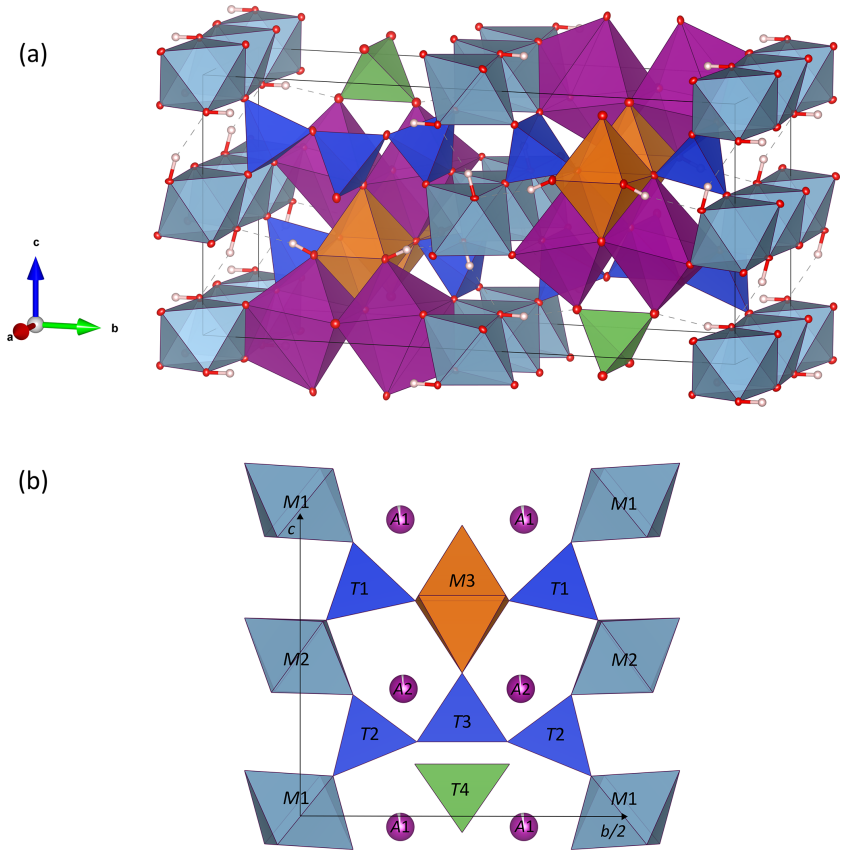

Figure 3. Crystal structure of ardennite-(As) from Regné (sample REGN-1). **(a)** General view of the structure, in which the H atoms are white spheres, AlO_6 octahedra are light blue, $A1O_6$ and $A2O_7$ polyhedra are purple, $M3O_6$ octahedra are orange, SiO_4 tetrahedra are dark blue, and $T4O_4$ tetrahedra are green. **(b)** View of the structure parallel to the *b*–*c* plane. Drawings were created with the VESTA 3 program (Momma and Izumi, 2011).

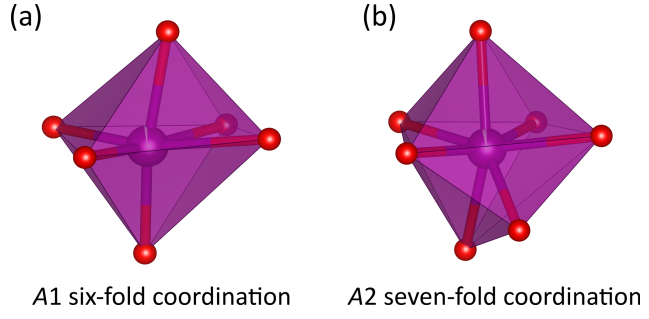

Figure 4. Morphologies of the $A1O_6$ **(a)** and $A2O_7$ **(b)** polyhedra in the crystal structure of ardennite-(As) from Regné. Drawings were created with the VESTA 3 program (Momma and Izumi, 2011).

by considering the multiplicity of each crystallographic site are in good agreement with the chemical compositions obtained from electron-microprobe analyses (Table 5).

OH groups of the ardennite structure were first located from a bond valence analysis (Donnay and Allmann, 1968), and the occurrence of hydrogen bonds was suggested by Pasero et al. (1994) to explain weak bond valence sums. Nagashima and Armbruster (2010) directly located the three hydrogen atoms, enabling a more accurate description of the H-bonding scheme of the ardennite structure. In the present

Table 6. Comparison of the O···H and O···H···O bond distances in ardennites. Calculated values were obtained from the wavenumbers measured on the infrared spectrum of sample TDP-1, using the empirical formula of Libowitzky (1999).

	TDP-1, this study	Nagashima and Armbruster (2010)	Calculated from IR spectrum
O10–H10	0.79	0.98	–
O10···O9	2.69	2.69	2.68
H10···O9	1.90	1.72	1.75
O11–H11	0.81	0.98	–
O11···O10	2.69	2.7	2.68
H11···O10	1.91	1.74	1.75
O12–H12	0.83	0.98	–
O12···O11	2.80	2.81	2.72
H12···O11	1.98	1.84	1.82

study, high-quality refinements performed on all samples except BIHN-1 and SALM-3 also allowed us to determine the exact location of the hydrogen atoms (Table S1); their positions are consistent with those of Nagashima and Armbruster (2010) and with those observed in the other minerals of the ardennite group (Kampf et al., 2017; Nishio-Hamane et al., 2018). O10, O11, and O12 act as donors, whereas O9, O10, and O11 act as acceptors of H bonds, indicating that O10 and O11 have a mixed donor–acceptor role. The hydrogen-bonding scheme in ardennite can then be summarized as follows: O10–H10···O9, O11–H11···O10, and O12–H12···O11. In our samples, the O–H distances range from 0.80 to 0.83 Å, the H···O distances from 1.88 to 1.98 Å, the O···O distances from 2.69 to 2.80 Å, and the O–H···O angle from 154 to 172° (Table 6). These results are relatively similar to those obtained by Kampf et al. (2017) in alpeite, while Nagashima and Armbruster (2010) restrained the O–H bond distances to 0.98 Å. Despite the weakness of the electrostatic attraction force, hydrogen bonds provide direct and non-direct (via $T4$ and $M3$) connections between the octahedral aluminium chains and then contribute to the overall stability of the structure.

6 The chemical composition of ardennites

At that stage, it is interesting to compare the general formula of ardennite-group minerals, $A_4^{2+}(M_5^{3+}M^{2+})(T_5^{4+}T^{5+})O_{22}(OH)_6$, with the formula obtained from the structural data, $A1_2A2_2(M1_2M2_2M3_2)(T1_2T2_2T3T4)O_{22}(OH)_6$. The occurrence of pentavalent cations on the $T4$ site implies the presence of divalent cations in the octahedral chains, according to the $^{T4}Si^{4+}+^{M3}(Al,Fe)^{3+} \leftrightarrow {}^{T4}(As,V,P)^{5+}+^{M3}Mg^{2+}$ substitution mechanism. However, the multiplicity of the $M3$ site is twice that of the $T4$ site, thus implying that only 50 % of the $M3$ positions have to be occupied by Mg^{2+}. Consequently, in the ideal end-member formulae of ardennite-group minerals, a valency-imposed double site occupancy on $M3$ is necessary to preserve charge balance (Hatert and Burke, 2008).

The electron-microprobe analyses (Table 1) show that several substitution mechanisms occur in the Belgian ardennite samples, leading to significant compositional variations. The A group of sites shows homovalent substitutions of Mn^{2+} by Ca^{2+} and Mg^{2+}, and because of its high ionic radius, Ca^{2+} has a strong preference for the larger $^{VII}A2$ site, where it can reach up to 0.48 apfu in sample SALM-1 and 0.33 apfu in sample CORX-1 (Table 1). Other ardennite samples show lower Ca contents mainly varying from 0.1 to 0.2 apfu; these small values are in good agreement with the geochemistry of the Ottré Formation, known to be depleted in calcium with CaO contents that rarely exceed 0.5 wt % (Depret et al., 2021). The slight Ca enrichment observed in some samples does not seem to be directly correlated with the mineralogical assemblages and could result from local variations. Another hypothesis would be the limited availability of manganese in the system due to the occurrence of Mn-bearing minerals (spessartine, braunite, strontiomelane) closely associated with ardennite grains and consequently leading to the incorporation of available calcium, rather than manganese, into the structure. Magnesium is preferentially incorporated in the $^{VI}A1$ site of the structure to balance the cationic deficit when the (Ca + Mn) content does not reach 4 apfu. The amount of Mg in $A1$ never exceeds 0.13 apfu (Table 1), and does not appear to be linked with a global increase in the Mg content in the sample.

The $M1$ and $M2$ octahedral sites only contain Al^{3+}, while $M3$ can simultaneously host Al^{3+}, Mg^{2+}, Mn^{3+}, and Fe^{3+}, as well as minor quantities of the divalent cations Ca, Mn^{2+}, Cu, and Zn (Table 1). In the Si-rich sample from Arbrefontaine (ARBR-1), significant amounts of V^{3+} were also considered on the $M3$ site, since the $T4$ site had already been filled with Si, As, and V^{5+}. This unusual sample will be further described below.

According to the valency-imposed double site occupancy due to the $^{T4}Si^{4+}+^{M3}(Al,Fe)^{3+} \leftrightarrow {}^{T4}(As,V,P)^{5+}+^{M3}Mg^{2+}$ substitution mechanism, the $M3$ site should ideally contain 50 % Mg^{2+} and 50 % trivalent cations (Al, Fe, Mn)$^{3+}$. The good correlation between ($^{T4}Si^{4+}+^{M3}R^{3+}$) and ($^{T4}R^{5+}+{}^{M3}R^{2+}$), with a slope close to −1 and a correlation coefficient of 0.97 (Fig. 5a), confirms that this mechanism is the main heterovalent substitution that occurs in ardennites. Pasero et al. (1994) described Belgian ardennites as Mg-poor and Al-rich, since they observed that the R^{2+}/R^{3+} ratio in $M3$ differs from 1; a modification of the OH^- content was therefore necessary to maintain charge balance. We did not observe such a feature and conclude that the low Mg contents of Belgian ardennites could be related to the relatively low MgO concentration of the host rocks (< 2 wt %; Depret et al., 2021) and/or to the strong competition with clinochlore.

The presence of Mn^{3+}, in concentrations reaching 0.12 apfu, has been observed in three samples found in the Meuville Member, which is more oxidized (log(fO_2) −7 to −2 bar) than the Les Plattes Member (log(fO_2) −24 to −6 bar; Gabelica, 2022). The Fe^{3+} content is quite similar in all ardennites (∼ 0.1 apfu), except in the red sample SALM-3, in which this element reaches 0.23 apfu; such an enrichment is certainly due to the close petrographic association with hematite. Cu and Zn are minor elements that occur in concentrations never exceeding 0.02 apfu (Table 1).

The main substitution affecting the $T4$ tetrahedral site is the $As^{5+} \leftrightarrow V^{5+}$ homovalent mechanism (Fig. 5b), but the electron-microprobe analyses also indicated the presence of smaller amounts of P^{5+} (< 0.28 apfu), Si^{4+} (< 0.10 apfu except in sample ARBR-1), and Al^{3+} (< 0.12 apfu) on that site (Table 1). Bermanec et al. (2021) compiled chemical data from the literature and concluded that the As–V solid solution was never complete in ardennites. Due to the close ionic radii of As^{5+} and V^{5+}, these authors considered geochemical

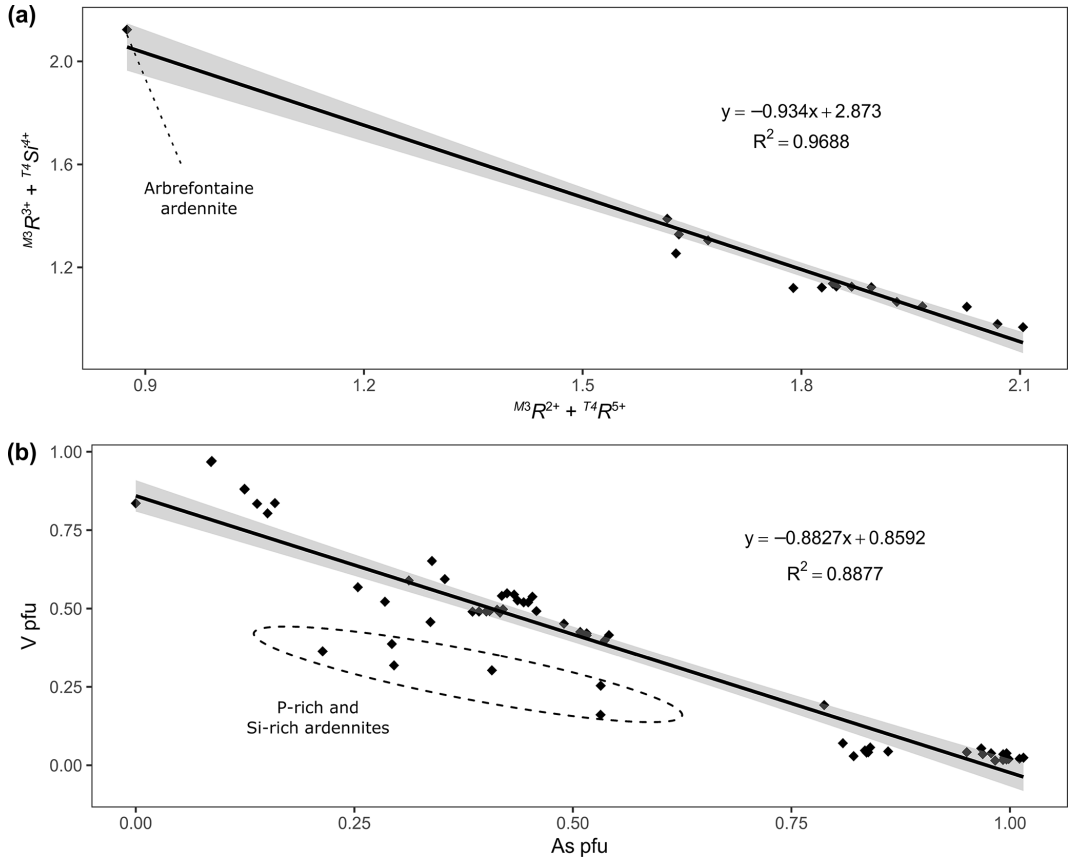

Figure 5. **(a)** Correlation between $\left({}^{M3}R^{3+} + {}^{T4}\mathrm{Si}^{4+}\right)$ and $\left({}^{M3}R^{2+} + {}^{T4}R^{5+}\right)$ in Belgian ardennite samples. **(b)** Correlation between the V and As contents (apfu) in Belgian ardennites.

factors rather than crystal-chemistry constraints to explain this miscibility gap. The new analyses of the present study, however, clearly show a continuous range of compositions between the As- and the V-bearing end-members (Fig. 5b), thus indicating a complete As–V solid solution confirmed by old data from the literature (Fig. 6). Electron-microprobe analyses of the samples TDM-1, BIHN-2, and OTTR-1 also revealed the existence of chemical zonations in some grains, characterized by wide variations in the As, V, and P contents (Table 1). Pasero et al. (1994) explained such small-scale variations by local compositional inhomogeneities of the sediments.

The P contents of ardennites are relatively low ($<$ 0.1 apfu) in most samples, showing that the substitutions on the $T4$ site mainly involve As and V. An As-rich sample from Regné (REGN-1) shows a significant P enrichment ($\sim$ 0.14 apfu) and a very low V content (0.05 apfu), indicating a limited solid solution along the As–P join (Fig. 6a). Other ardennite samples characterized by intermediate As–V compositions may show more important P incorporations (up to 0.28 apfu in sample OTTR-1b; Fig. 6a); however, in these samples, P enrichments are variable and seem to be strongly associated with heterogenous zonations. The much smaller ionic radius of P^{5+} (0.17 Å; Shannon, 1976), compared to those radii of As^{5+} and V^{5+} (0.335 and 0.355 Å, respectively), is probably the main factor governing the limited incorporation of P in the ardennite structure. These crystal-chemistry constraints are combined with the limited availability of P in the rocks ($<$ 0.5 wt %; Depret et al., 2021) and/or with strong competition with associated phosphate minerals. Higher P contents have been observed in ardennites from high-pressure metamorphic rocks (Pasero et al., 1994) and result from an overall contraction of the structure that favoured P incorporation.

The only significant occurrences of Si in the $T4$ site are observed in samples OTTR-1a and OTTR-1b (Table 1; Fig. 6b), in which the excess of Si is used to balance the deficit in pentavalent cations ($\mathrm{As} + \mathrm{V} + \mathrm{P} \sim 0.88$ apfu). Analyses made on ardennites from Vitolište, North Macedonia (Altherr et al., 2017), suggest the existence of a complete Si–V solid solution. However, this solid solution may in fact be relatively restricted because intermediate members, as well as ardennite-(Si) compositions, may be produced by tiny intergrowths of lavoisierite $[Mn_8^{2+}Al_{10}(Mn^{3+}Mg)Si_{11}PO_{44}(OH)_{12}]$, an ardennite polysome containing ardennite- and sursassite-like slabs

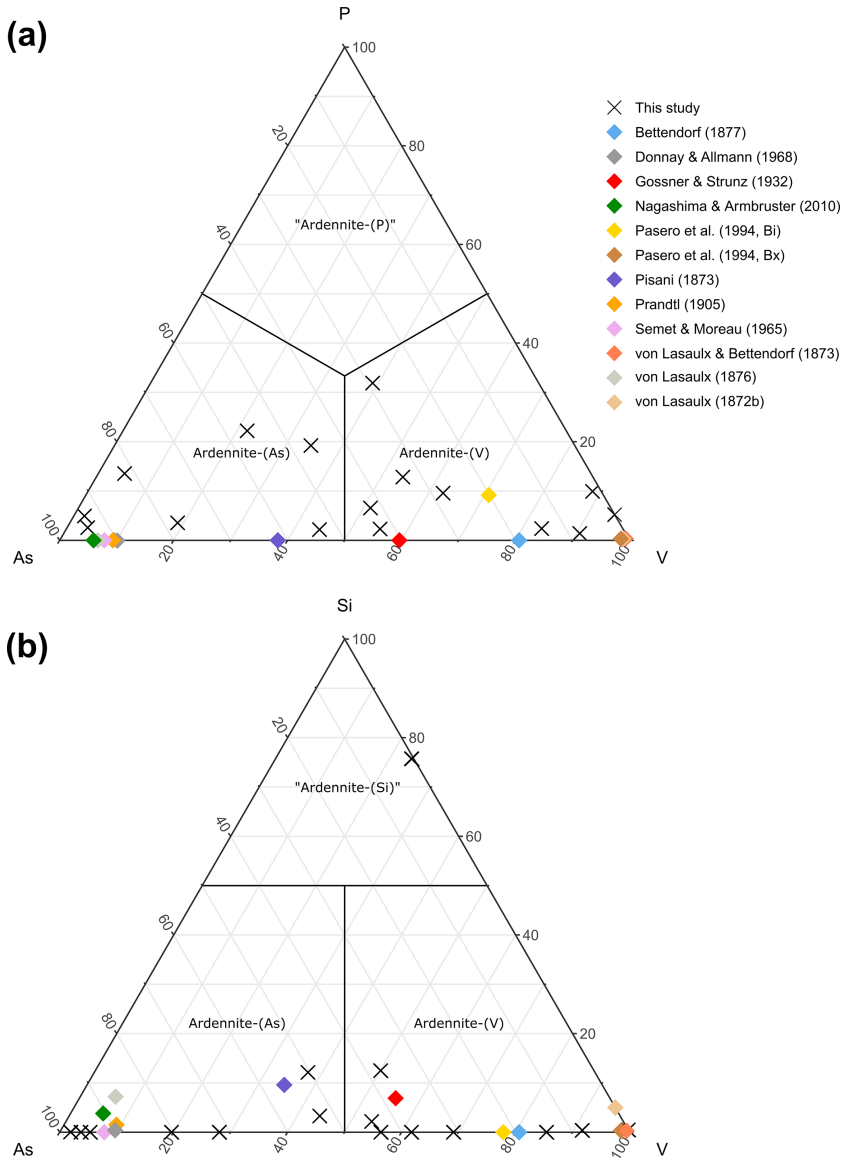

Figure 6. Ternary As–P–V **(a)** and As–Si–V **(b)** diagrams, showing compositional variations on the $T4$ site of ardennites.

and a doubled c parameter (Orlandi et al., 2013). Due to the small size of the grains, no X-ray diffraction analyses could be performed to determine the real nature of the mineral. Finally, an unusual ardennite sample was collected at Arbrefontaine (sample ARBR-1), which shows an important enrichment in Si with a high V content (Fig. 6b). According to the procedure described by Nagashima and Armbruster (2010), when the sum of tetra- and pentavalent cations on the T sites exceeds 6 apfu, the excess of V is assigned to the octahedral $M1$ or $M3$ sites as V^{3+}. From an average of nine electron-microprobe analyses, we consequently obtain the empirical formula $(Mn^{2+}_{3.77}Ca_{0.18}Mg_{0.05})\Sigma_{4.00}(Al_{4.60}V^{3+}_{0.70}Mg_{0.60}Fe^{3+}_{0.09}Cu^{2+}_{0.01})_{\Sigma 6.00}(Si)_{\Sigma 5.00}(Si_{0.74}V^{5+}_{0.23}P_{0.03})_{\Sigma 1.00}]O_{22}(OH)_{5.65}$ for the sample ARBR-1 (Table 1). This phase may correspond to a new Si- and V^{3+}-rich end-member of the ardennite group, but further crystal structure characterizations are necessary to confirm this hypothesis.

7 Infrared spectroscopy

Infrared spectral measurements were performed on the two ardennite samples CORX-1 and TDP-1, and both spectra are relatively similar (Fig. 7). In the 800–1200 cm^{-1} region, complex overlapping bands occur, mainly dominated by SiO_4 and Si_3O_{10} vibration modes (Frost et al., 2014). The band at 1114 cm^{-1} corresponds to the Si–O antisymmetric stretching vibrations, and the group of bands between 1022 and 835 cm^{-1} can be assigned to the Si–O stretching

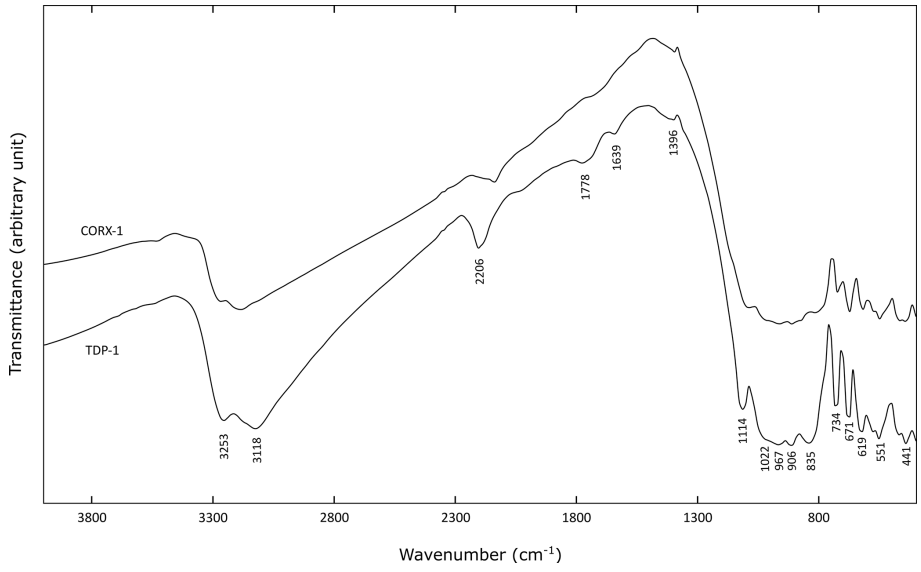

Figure 7. Infrared spectra of the CORX-1 and TDP-1 ardennite samples.

and bending vibrations. Below 800 cm^{-1}, several bands corresponding to tetrahedral bending modes, as well as to lattice vibrations, occur.

Between 3100 and 3300 cm^{-1}, large bands attributed to O–H stretching vibrations occur. Two peaks can be distinguished at 3118 and 3253 cm^{-1} (Fig. 7), which are produced by various cationic coordination of the oxygens involved in hydroxyl groups. Indeed, O10 and O11 are linked to the two neighbouring Al atoms, while O12 is surrounded by Mg and Mn, thus leading to the splitting of the O–H stretching frequencies. O–H···O distances, calculated with the empirical equation of Libowitzky (1999), are relatively close to those obtained from our structure refinements, while the calculated H···O bond lengths seem to be significantly smaller (Table 6). In their study, Nagashima and Armbruster (2010) constrained the O–H bond distances to 0.98 Å, leading to shorter H···O bond lengths that were more consistent with the infrared data (Table 6). Our O–H bond lengths are probably slightly underestimated. A weak band at 1639 cm^{-1}, corresponding to the bending vibrational mode of water molecules, has also been observed in the spectrum of sample TDP-1 (Fig. 7). This indicates that small amounts of water could be incorporated in the structure or absorbed on the ardennite surface, as suggested by Frost et al. (2014).

8 Discussion

8.1 Crystal chemistry of ardennite-group minerals

A comparison of the unit-cell parameters of ardennites (Table 2) with the compositional data (Table 1) indicates that the unit-cell volume is significantly higher in Ca-rich samples. Positive correlations were consequently observed between the (Ca + Mg + Fe) contents of ardennites and their unit-cell parameters (Fig. 8). The absence of good correlations between the As / V ratio and the unit-cell parameters can certainly be explained by the very close ionic radii of As and V of 0.335 and 0.355 Å, respectively (Shannon, 1976).

The increase in the unit-cell parameters with the (Ca + Mg + Fe) contents of ardennites is induced by two independent substitution mechanisms: the replacement of Al by Fe^{3+} and Mg on the $M3$ site (Mg is introduced into the structure via the coupled heterovalent substitution mechanism described above) and the replacement of Mn^{2+} by Ca on the $A2$ site. Indeed, Fe^{3+} (the effective ionic radius, eir, is 0.645 Å) and Mg (eir = 0.72 Å) show larger ionic radii than Al (eir = 0.535 Å), and Ca (eir = 1.06 Å) shows a larger ionic radius than Mn^{2+} (eir = 0.90 Å; Shannon, 1976). It is important to underline that the a unit-cell parameter variation shows a slope of ca. 0.01, significantly lower than the slopes of the correlations involving b and c, both close to 0.03 (Fig. 8). This feature can be explained by the presence of chains of edge-sharing AlO_6 octahedra aligned along the a axis, which are formed by the $M1$ and $M2$ sites not affected by any substitution. These chains, therefore, act as rigid units maintaining the a values relatively constant.

We also attempted to correlate the chemical composition and the structural parameters of ardennites, but only a few satisfactory trends were observed, probably due to an overall adjustment of the unit cell as a result of the different substitution mechanisms occurring in those minerals. As shown in Fig. 9, a satisfactory correlation was nevertheless observed between the mean bond lengths of the $T4$ and $M3$ sites (Table 4), on which the most significant substitutions occur, and the bond lengths calculated from the assigned site populations on those sites (Table 5) and from the ideal ionic radii of

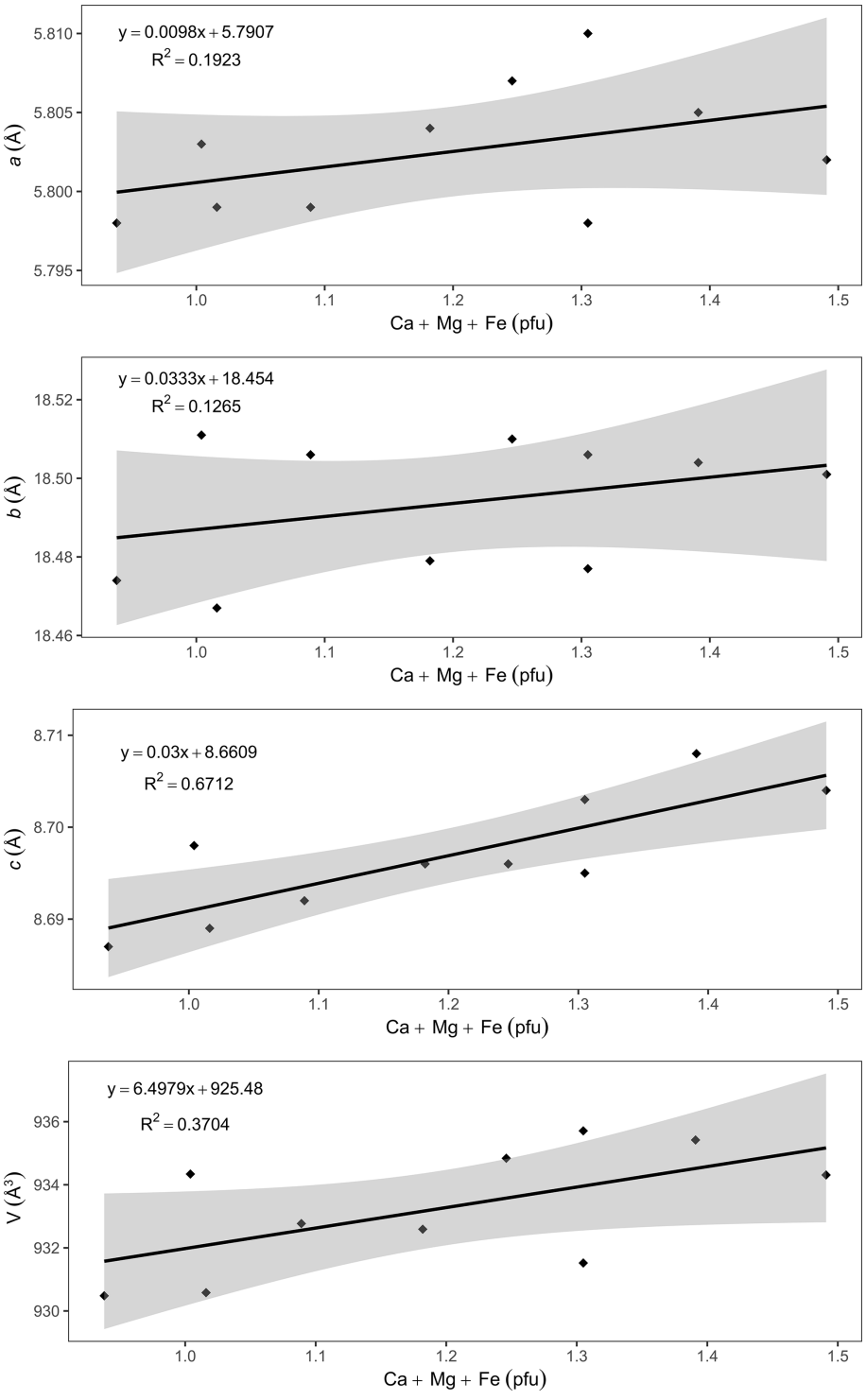

Figure 8. Variations in the unit-cell parameters of Belgian ardennites, with their (Ca + Mg + Fe) contents (pfu).

Shannon (1976). These correlations confirm the reliability of the assigned site populations.

A negative correlation has also been observed between the bond length distortion coefficients of the $M3$ and $T4$ sites (Fig. 10), which seems to be controlled by the position of O5, shared by the two cations (Fig. 3). Both sites are prone to heterovalent substitutions (Al by Mg or As^{5+}, V^{5+} by Si^{4+}), and O5 moves closer to either of the cations according to the mean charge balance in each site. Since our samples show a very limited incorporation of Si^{4+} in the $T4$ site, the overall

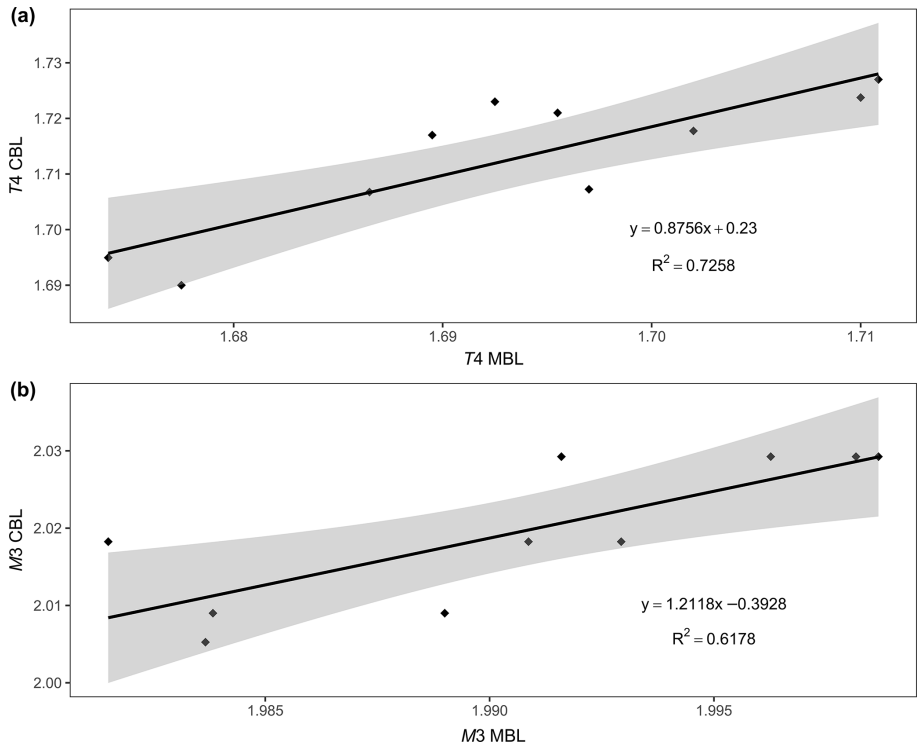

Figure 9. Correlations between the calculated bond length (CBL) and the mean bond length (MBL) values, for the $T4$ **(a)** and $M3$ **(b)** crystallographic sites of Belgian ardennites.

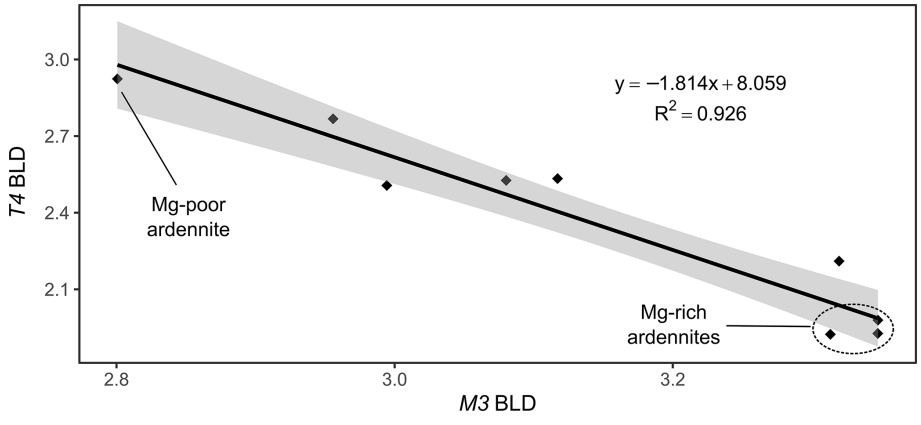

Figure 10. Correlation between the bond length distortion (BLD) parameters of the $T4$ and $M3$ sites of the ardennite structure.

valence of $M3$ decreases as the Mg content increases, and O5 then gets closer to $T4$ and vice versa.

8.2 Hypothetical existence of P- and Si-rich end-members

While the As–V homovalent substitution mechanism allows the existence of a complete solid solution between ardennite-(As) and ardennite-(V) (Figs. 5b, 6), the incorporation of Si^{4+} and P^{5+} on the $T4$ site of the ardennite structure seems to be more restricted.

The homovalent substitution of As^{5+} and V^{5+} by P^{5+} implies that the boundaries between ardennite-(As), ardennite-(V), and the potential new species "ardennite-(P)" are located at 33.3 %, as shown in Fig. 6a. Pasero et al. (1994) discussed the crystal chemistry of phosphorus in ardennites in detail and concluded that the samples richest in P were produced in high-pressure environments. Moreover, they observed a positive correlation between the phosphorus contents of ardennites and the Mg contents on the $A1$ site. Such a correlation is not obvious in the Belgian samples investigated in the present paper, since the compositions richest in P (REGN-1, BIHN-

2a and BIHN-2b, OTTR-1a and OTTR-1b; Table 1) do not necessarily contain significant amounts of Mg on the *A* sites.

Pasero et al. (1994) explain that all attempts to synthesize P-rich ardennites under high-pressure conditions failed and produced assemblages containing ellenbergerite or phosphoellenbergerite (Brunet et al., 1998). These authors concluded that P-rich ardennite would be unstable relative to P-rich ellenbergerite, thus reducing the possible P contents of ardennites below 0.5 apfu. However, the data presented in our study clearly show that, even under the low-*P*, low-*T* conditions prevailing in the Stavelot Massif, ardennites occur with P contents reaching 0.28 P apfu (Table 1, Fig. 6a). The hypothetical species "ardennite-(P)" would therefore be stable in any type of low-pressure environment, depending on local P enrichments, and without any competition with high-pressure ellenbergerite-type phases. The only limitations, possibly restricting P incorporation in the ardennite structure, are the crystal-chemistry constraints, but the exact extent of the possible solid solutions is extremely difficult to estimate.

The replacement of pentavalent As^{5+} and V^{5+} by tetravalent Si^{4+} is heterovalent and consequently necessitates the coupled substitution of Mg^{2+} by Al^{3+} on the *M*3 site, as described above. As a consequence of this heterovalent substitution, the dominant-valency rule must be applied (Hatert and Burke, 2008), and the boundaries on the ternary diagram of Fig. 6b are moved slightly upwards, since more than 50 % Si^{4+} pfu on *T*4 is necessary to obtain the potential new species "ardennite-(Si)".

Most analyses of ardennites from the Stavelot Massif contain less than 0.1 Si pfu on the *T*4 site (Fig. 6b), but this amount can easily exceed 0.2 apfu in samples from Greece and the Western Alps (Pasero et al., 1994), as well as in samples from North Macedonia (Altherr et al., 2017). Pasero et al. (1994) indicate that the Si contents of their samples are highly variable from one point to another in the thin sections, suggesting a fine intergrowth of ardennite with another Si-rich mineral. High-resolution transmission electron-microscopic studies by Pasero and Reinecke (1991) on those samples indicate an intergrowth of "normal" ardennite domains with a phase characterized by $c = 37$ Å; this phase was later described as lavoisierite (Orlandi et al., 2013).

The electron-microprobe analyses of sample ARBR-1 from Arbrefontaine (Table 1, Fig. 6b) indicate close to 0.74 Si pfu on the *T*4 site; this sample would therefore correspond to the new species "ardennite-(Si)". However, preliminary structure refinements do not confirm the dominance of Si on *T*4, thus preventing the definition of this species. Further investigations are needed to confirm the status of that phase, but at the present stage, the occurrence of lavoisierite-type domains in sample ARBR-1 cannot be ruled out.

8.3 Nomenclature of the ardennite group

In the present paper, we have reinterpreted the old analytical data on ardennites on the basis of 16 cations pfu in order to evaluate their validity. In their early analyses, von Lasaulx (1872b) and von Lasaulx and Bettendorf (1873) did not find the presence of As in the mineral; however, the V contents were close to 1 apfu (0.95 and 1.04 V pfu, respectively), thus indicating that the first investigated samples certainly corresponded to ardennite-(V). Pisani (1873) first identified arsenic in the mineral, and his sample, as well as those later analysed by von Lasaulx (1876) and Prandtl (1905), corresponds to ardennite-(As). Bettendorf (1877), as well as Gossner and Strunz (1932), unambiguously identified two samples in which V was dominant over As, confirming the existence of a vanadium-rich "variety" of ardennite in Salmchâteau (Fig. 6). More recently, two analyses from Bierleux and Bihain were published by Pasero et al. (1994) that correspond to ardennite-(V), and the analyses given in the present paper (Table 1, Fig. 6) clearly indicate the occurrence of both ardennites in the Stavelot Massif.

In their paper describing the new species ardennite-(V), Barresi et al. (2007) argued that most old analyses were doubtful, and the authors consequently defined the species with its type locality at Sparone, Piedmont, Italy. However, our reinterpretation of the old analyses clearly indicates that both species, ardennite-(As) and ardennite-(V), were originally present at Salmchâteau or in the area, thus raising the question of the legitimacy of the type locality for ardennite-(V). We suggest a modification of the type locality for ardennite-(V), which should also be Salmchâteau. We are currently preparing a IMA CNMNC (International Mineralogical Association – Commission on New Minerals, Nomenclature and Classification) proposal for this nomenclature change, and we will define the V-rich sample SALM-2 as the neotype.

The existence of both species in the original samples from Salmchâteau is certainly at the origin of the disagreement between A. von Lasaulx and F. Pisani, who decided to give different names to these minerals. Ardennite was named by von Lasaulx (1872a) for the Ardennes mountains where the mineral was found, and dewalquite was named by Pisani (1873) for the famous Belgian geologist Gustave Dewalque of the University of Liège (1826–1905; Anceau et al., 2017). Nowadays, only the name ardennite is retained by the CNMNC, even if some old labels in the collections of the University of Liège still mention dewalquite (Fig. 2a).

Our last nomenclature suggestion for the ardennite group concerns the revalidation of dewalquite. Indeed, since the early samples of the V-rich variety were named ardennite by von Lasaulx (1872a), and since the presence of arsenic was first demonstrated by Pisani (1873) on samples that he named dewalquite, it seems logical to rename ardennite-(V) as ardennite and ardennite-(As) as dewalquite. However, if a suffix-based nomenclature is preferred for the group (Hatert

et al., 2013), we could define dewalquite as a new root-name, corresponding to a V^{3+}- and Si-rich species such as sample ARBR-1 (Table 1). These decisions, however, have to pass through the CNMNC for validation.

Data availability. All data are available upon request to Martin Depret.

Supplement. The supplement related to this article is available online at: https://doi.org/10.5194/ejm-36-687-2024-supplement.

Author contributions. The samples investigated herein were discovered in the field by MB and SP. The electron-microprobe analyses were performed by MMLE, and the single-crystal structure refinements were conducted by MD. The manuscript was written by MD and FH and corrected by FDB and FB.

Competing interests. The contact author has declared that none of the authors has any competing interests.

Disclaimer. Publisher's note: Copernicus Publications remains neutral with regard to jurisdictional claims made in the text, published maps, institutional affiliations, or any other geographical representation in this paper. While Copernicus Publications makes every effort to include appropriate place names, the final responsibility lies with the authors.

Acknowledgements. Many thanks are due to Nicolas Delmelle, who helped us with the infrared spectral measurements, and to the reviewers for their constructive comments.

Review statement. This paper was edited by Rucheng Wang and reviewed by Łukasz Kruszewski and two anonymous referees.

References

Altherr, R., Soder, C., Meyer, H.-P., Ludwig, T., and Böhm, M.: Ardennite in high – P/T meta – conglomerate near Vitolište in the westernmost Vardar zone, Republic of Macedonia, Eur. J. Mineral., 29, 473–489, 2017.

Anceau, A., Prestiani, C., Hatert, F., and Denayer, J.: Les sciences géologiques à l'Université de Liège : deux siècles d'évolution. Partie 1 : de la fondation à la Première Guerre Mondiale, Bulletin de la Société Royale des Sciences de Liège, 86, 27–101, 2017.

Baijot, M., Hatert, F., and Fransolet, A.-M.: Mineralogical and geochemical study of pseudocoticule from the Stavelot Massif, Ardennes (Belgium), and redefinition of coticule, Can. Mineral., 23, 633–644, 2011.

Barresi, A. A., Orlandi, P., and Pasero, M.: History of ardennite and the new mineral ardennite-(V), Eur. J. Mineral., 19, 581–587, 2007.

Bermanec, M., Chukanov, N. V., Boev, I., Šturman, B. D., Zebec, V., and Bermanec, V.: Ardennite-bearing mineral association related to sulfide-free ores with chalcophile metals at Nežilovo, Pelagonian Massif, North Macedonia, Eur. J. Mineral., 33, 433–445, https://doi.org/10.5194/ejm-33-433-2021, 2021.

Bernhardt, H.-J., Armbruster, T., Fransolet, A.-M., and Schreyer, W.: Stavelotite-(La), a new lanthanum-manganese-sorosilicate from the Stavelot Massif, Belgium, Eur. J. Mineral., 17, 703–714, 2005.

Bettendorf, A.: Ueber den Ardennit und über eine Methode zur Schneidung der Vanadinsaüre von Thonerde und Eisenoxyd, Ann. Chim. Phys., 160, 126–131, 1877.

Blondieau, M., Puccio, S., Compère, P., and Hatert, F.: Données nouvelles sur quelques espèces minérales de Vielsalm et de Salmchâteau (Province de Luxembourg, Belgique), Bulletin de la Société Royale des Sciences de Liège, 86, 1–48, 2017.

Brown, I. D. and Altermatt, D.: Bond-valence parameters obtained from a systematic analysis of the Inorganic Crystal Structure Database, Acta Crystallogr., B41, 244–247, 1985.

Brunet, F., Chopin, C., and Seifert, F.: Phase relations in the MgO–P_2O_5–H_2O system and the stability of phosphoellenbergerite: petrological implications, Contrib. Mineral. Petr., 131, 54–70, 1998.

Bultynck, P. and Dejonghe, L.: Devonian lithostratigraphic units (Belgium), Geol. Belg., 4, 39–69, 2001.

Cesàro, G. and Abraham, A.: La dewalquite, Annales de la Société Géologique de Belgique, 36, 197–212, 1909.

Corin, F.: Contribution à l'étude de la dewalquite, Annales de la Société Géologique de Belgique, 51, 140–144, 1927.

Dal Piaz, G. V., Di Battistini, G., Kienast, J.-R., and Venturelli, G.: Manganesiferous quartzitic schists of the Piemonte ophiolite nappe, Mem. Sc. Geol. Padova, 32, 1–24, 1979.

Depret, M., Bruni, Y., Dassargues, A., Defourny, A., Marion, J.-M., Vanderschueren, W., and Hatert, F.: Mineralogical and hydrogeological study of "pouhons" in the lower Paleozoic formations of the Stavelot-Venn Massif, Geol. Belg., 24, 109–124, 2021.

Dolomanov, O. V., Blake, A. J., Champness, N. R., and Schröder, M.: OLEX: new software for visualization and analysis of extended crystal structures, J. Appl. Crystallogr., 36, 1283–1284, 2003.

Donnay, G. and Allmann, R.: Si_3O_{10} groups in the crystal structure of ardennite, Acta Crystallogr., B24, 845–855, 1968.

Ferket, H., Muchez, P., Schroyen, K., and Sintubin, M.: Metamorphism in the Stavelot-Venn Massif: a study of quartz veins in the Devonian conglomerates (Lochkovian), Aardkundinge Mededelingen, 9, 7–16, 1998.

Fielitz, W. and Mansy, J.-L.: Pre- and synorogenic burial metamorphism in the Ardenne and neighbouring areas (Rhenohercynian zone, central European Variscides), Tectonophysics, 309, 227–256, 1999.

Fransolet, A.-M.: Minéralogie de Belgique, Ardennite, Bulletin de la Société Belge de Géologie, 91, 50, 1982.

Frost, R. L., López, A., Xi, Y., Scholz, R., and Gandini, A. L.: A vibrational spectroscopy study of the silicate mineral ardennite – (As), Spectrochim. Acta, A118, 987–991, 2014.

Geukens, F.: Commentaire à la carte géologique du Massif de Stavelot, Aarkundinge Mededelingen, 3, 15–30, 1986.
Geukens, F.: Notes accompagnant une révision de la carte structurale du Massif de Stavelot, Aardkundinge Mededelingen, 9, 183–190, 1999.
Gabelica, D.: Etude minéralogique, pétrographique et géochimique de la Formation d'Ottré, Massif de Stavelot, Master Thesis, University of Liège, 2022.
Goemaere, E.: Ardoise et coticule en Terre de Salm: des pierres et des hommes, Service Géologique de Belgique, 408 p., 2007.
Gossner, B. and Strunz, H.: Ueber strukturelle Beziehungen zwischen Phosphaten (Triphylin) und Silikaten (Olivin) und über die chemische Zusammensetzung von Ardennit, Z. Kristallogr., 83, 415–421, 1932.
Hatert, F.: Etude minéralogique préliminaire de quelques sulfures du Massif de Stavelot, Master Thesis, University of Liège, 1996.
Hatert, F.: Occurrence of sulphides on the bornite-idaite join from Vielsalm, Stavelot Massif, Belgium, Eur. J. Mineral., 15, 1063–1068, 2003.
Hatert, F.: Transformation sequences of copper sulphides at Vielsalm, Stavelot Massif, Belgium, Can. Mineral., 43, 623–635, 2005.
Hatert, F. and Burke, E. A. J.: The IMA-CNMNC dominant-constituent rule revisited and extended, Can. Mineral., 46, 717–728, 2008.
Hatert, F., Deliens, M., Fransolet, A.-M., and Van Der Meersche, E.: Les Minéraux de Belgique, Deuxième édition, Bietlot, Gilly, 304 pp., 2002.
Hatert, F., Fransolet, A.-M., Wouters, J., and Bernhardt, H.-J.: The crystal structure of sursassite from the Lienne valley, Stavelot Massif, Belgium, Eur. J. Mineral., 20, 993–998, 2008.
Hatert, F., Mills, S. J., Pasero, M., and Williams, P. A.: CNMNC guidelines for the use of suffixes and prefixes in mineral nomenclature, and for the preservation of historical names, Eur. J. Mineral., 25, 113–115, 2013.
Hatert, F., Blondieau, M., Puccio, S., Baijot, M., and Gustine, C.: Le gisement de manganèse de la Vallée de la Lienne, Belgique, Le Règne Minéral, 117, 5–24, 2014.
Herbosch, A., Liégeois, J.-P., and Pin, C.: Coticules of the Belgian type area (Stavelot-Venn Massif): Limy turbidites within the nascent Rheic oceanic basin, Earth-Sci. Rev., 159, 186–214, 2016.
Kampf, A. R., Carbone, C., Belmonte, D., Nash, B. P., Chiappino, L., and Castellaro, F.: Alpeite, $Ca_4Mn_2^{3+}Al_2(Mn^{3+}Mg)(SiO_4)_2(Si_3O_{10})(V^{5+}O_4)(OH)_6$, a new ardennite-group mineral from Italy, Eur. J. Mineral., 29, 907–914, 2017.
Kramm, U.: The coticule rocks (spessartine-quartzites) of the Venn-Stavelot Massif, Ardennes, a volcanoclastic metasediment?, Contrib. Miner. Petrol., 56, 135–155, 1976.
Kramm, U.: Die Metamorphose des Venn-Stavelot-Massivs, nordwestliches Rheinisches Schiefergebirge: Grad, Alter und Ursache, Decheniana, 135, 121–178, 1982.
Kramm, U., Spaeth, G., and Wolf, M.: Variscan metamorphism in the NE Stavelot-Venn Massif, Ardennes: A new approach to the question of regional dynamothermal or contact metamorphism, Neues Jahrbuch für Geologie und Paläontologie, Abhandlungen, 171, 311–327, 1985.
Krosse, S. and Schreyer, W.: Comparative geochemistry of coticules (spessartine-quartzite) and their redschist country rocks in the Ordovician of the Ardennes Mountains, Belgium, Chemie der Erde, 53, 1–20, 1993.
Lessuise, A.: Le coticule: situation géographique et géologique des gisements. Exploitation et préparation des pierres abrasives. Valorisation des déchets d'exploitation. INIEX-NIEB, Département mines et carrières, Liège, 37 pp., 1980.
Libowitzky, E.: Correlation of O-H Stretching Frequencies and O-H O Hydrogen Bond Lengths in Minerals, Monatshefte für Chemie, 130, 1047–1059, 1999.
Momma, K. and Izumi, F.: VESTA 3 for three-dimensional visualization of crystal, volumetric and morphology data, J. Appl. Crystallogr., 44, 1272–1276, 2011.
Nagashima, M. and Armbruster, T.: Ardennite, tiragalloite and mediate: structural control of $(As^{5+},V^{5+},Si^{4+})O_4$ tetrahedra in silicates, Mineral. Mag., 74, 55–71, 2010.
Nayak, V. K.: Ardennites from Kajilidongri, India: a new locality, Neues Jb. Miner. Monat., 1967, 295–304, 1967.
Nishio-Hamane, D., Nagashima, M., Ogawa, N., and Minakawa, T.: Kannanite, a new mineral from Kannan Mountain, Japan, J. Miner. Petrol. Sci., 113, 245–250, 2018.
Orlandi, P., Biagioni, C., Pasero, M., and Mellini, M.: Lavoisierite, $Mn[Al_{10}(Mn^{3+}Mg)][Si_{11}P]O_{44}(OH)_{12}$, a new mineral from Piedmont, Italy: the link between "ardennite" and sursassite, Phys. Chem. Miner., 40, 239–249, 2013.
Oxford Diffraction: Crys Alis PRO, Oxford Diffraction Ltd, Abingdon, Oxfordshire, England, 2007.
Pasero, M. and Reinecke, T.: Crystal chemistry, HRTEM analysis and polytypic behaviour of ardennite, Eur. J. Mineral., 3, 819–830, 1991.
Pasero, M., Reinecke, T., and Fransolet, A.-M.: Crystal structure refinements and compositional control of Mn-Mg-Ca ardennites from the Belgian Ardennes, Greece, and the Western Alps, Neues Jb. Miner. Abh., 166, 137–167, 1994.
Pisani, F.: Sur un nouveau silico-aluminate de manganese vanadifère, trouvé à Salm Château, en Belgique, Comptes-Rendus de l'Académie des Sciences de Paris, 75, 1542–1544, 1872.
Pisani, F.: Analyse de la dewalquite de Salm-Château en Belgique, Comptes-Rendus de l'Académie des Sciences de Paris, 77, 329–333, 1873.
Prandtl, W.: Ueber den Ardennit, Zeitschrift für Kristallographie und Mineralogie, 40, 392–395, 1905.
Reinecke, T. and Hatzipanagiotou, K.: Crystal chemistry and lattice parameters of ardennites from Andros Island, Greece, and Haute-Maurienne, Western Alps, Neues Jb. Miner. Abh., 158, 89–104, 1987.
Schreyer, W.: New petrologic evidence for Hercynian metamorphism in the Venn-Stavelot Massif, Belgium, Geol. Rundsch., 64, 819–830, 1975.
Semet, M. and Moreau, J.: L'ardennite: révision et données nouvelles, Annales de la Société Géologique de Belgique, 88, 545–577, 1965.
Shannon, R. D.: Revised effective ionic radii and systematic studies of interatomic distances in halides and chalcogenides, Acta Crystallogr., A32, 751–767, 1976.
Sheldrick, G. M.: A short history of SHELX, Acta Crystallogr., A64, 112–122, 2008.

Theye, T., Schreyer, W., and Fransolet, A.-M.: Low-temperature, low-pressure metamorphism of Mn-rich rocks in the Lienne syncline, Venn-Stavelot Massif (Belgian Ardennes), and the role of carpholite, J. Petrol., 37, 767–783, 1996.

Verniers, J., Herbosch, A., Vanguestaine, M., Geukens, F., Delcambre, B., Pingot, J.-L., Belanger, I., Hennebert, M., Debacker, T., Sintubin, M., and De Vos, W.: Cambrian-Ordovician-Silurian lithostratigraphic units (Belgium), Geol. Belg., 4, 5–38, 2001.

von Lasaulx, A.: Ardennit, ein neues Mineral, Neues Jahrbuch für Mineralogie, Geologie und Paläontologie, 930–934, 1872a.

von Lasaulx, A.: Über ein neues Mineral aus der Gegend von Ottrez. Sitzungsberichte der niederrheinischen Gesellschaft für Natur- und Heilkunde in Bonn, Verhandlungen des Naturhistorischen Vereines der Preussischen Rheinlande und Westphalens, 29, 189–192, 1872b.

von Lasaulx, A.: Nachträge zur Kenntniss des Ardennites, Neues Jahrbuch für Mineralogie, 1876, 363–368, 1876.

von Lasaulx, A. and Bettendorf, A.: Ardennit, ein neues Mineral, Ann. Chim. Phys., 149, 241–251, 1873.

Warr, L. N.: IMA-CNMNC approved mineral symbols, Mineral. Mag., 85, 291–320, 2021.

Wilson, A. J. C.: International Tables for X-ray Crystallography, Vol. C. Kluwer Academic Press, London, 883 pp., 1992.